UNIVERSITY OF AVEIRO
2014

DEPARTMENT OF MATERIALS AND CERAMICS ENGINEERING

ALEXANDRE MANUEL FERRO ROCHA

SCREENING AND DEVELOPMENT OF CORROSION INHIBITORS FOR Al ALLOYS

Dissertation submitted to University of Aveiro to accomplish the necessary requirements to obtain of a Master's degree in Materials Engineering. This work was carried out under the scientific guidance of Dr. Silvar Kallip, assistant researcher at the Department of Ceramics and Materials Engineering at the University of Aveiro.

"Nothing is enough for the man to whom enough is too little."

Epicurus

the jury

president

Prof. Doutor Mário G. S. Ferreira
Professor catedrático do Departamento de Engenharia de Materiais e Cerâmica da Universidade de Aveiro

Prof. Doutor Christopher M. A. Brett
Professor catedrático da Faculdade de Ciências e Tecnologia do Departamento de Química da Universidade de Coimbra

Doutor Silvar Kallip
Investigador Auxiliar do Departamento de Engenharia de Materiais e Cerâmica da Universidade de Aveiro

acknowledgements

Primarily, my biggest thank you goes to my family and girlfriend due to all the help and support they always gave me throughout my studies and especially during the time of this Thesis Preparation - without them none of this would have ever been possible.

Secondly, I would like to thank the Investigation Group (Professor Mário Ferreira, Alexandre Bastos, André Oliveira and others) that welcomed me, along with everyone in Smallmatek, Lda (João Tedim, Professora Maria Júlia, Nuno Nogueira, Francisco, Frederico, Cláudia, Eliana). They were always there to give me a helping hand and discuss any aspect I needed, anytime I needed. The way I was received by everyone is something that I will not forget. Thank you for giving me the opportunity to work with the best!

A special thank you to my friend and advisor Dr. Silvar Kallip. All the hours spent with me, all the explanations, all the help given, along with every conversation on different aspects and themes surely helped me to better achieve this final stage of my studies and to become a better student and person.

The last but not the least goes specifically to my friends (especially Daniel Vieira and Marco Oliveira). Thank you for our endless conversations in the last years of our course, they were very important for me to achieve this goal.

Smallmatek Lda and Smarmat OÜ are acknowledged for internship opportunity and electrochemical equipment availability.

The EU FP7 project PIAPP-GA-2013-612415 (PROAIR) and FCT Exploratory project IF/00856/2013/CP1162/CT0019 are greatly acknowledged for financial support.

palavras-chave Corrosão, Inibidores, Ligas de Alumínio, Concentração, EIS, SVET.

resumo

O objectivo deste trabalho foi procurar/pesquisar de forma sistemática os efeitos da corrosão em estruturas metálicas e ligas, bem como a protecção das mesmas a este fenómeno.

Devido às suas propriedades específicas (baixa densidade e boa resistência mecânica) e aplicações práticas em áreas como a aeronáutica, as ligas de alumínio foram os materiais estudados. Este estudo foi feito através do enquadramento e desenvolvimento de estratégias de inibição da corrosão, à superfície das ligas de alumínio seleccionadas, em condições de extensiva corrosão localizada.

A combinação e sistemática aplicação de técnicas de análise electroquímica - desde técnicas bem conhecidas de análise integral (EIS) a técnicas sofisticadas para análise localizada (SVET) - foram as ferramentas usadas para levar a cabo este estudo. As vantagens desta abordagem e da combinação de diferentes técnicas serão criticamente analisadas e avaliadas do ponto de vista da estimativa do comportamento corrosivo nas superfícies das diferentes ligas de alumínio quando em contacto com ambientes electrolíticos que contêm iões cloreto.

keywords Corrosion, Inhibitors, Aluminium alloys, Concentration, EIS, SVET.

abstract

The goal of this work was to systematically seek and study the corrosion and corrosion protection of metallic materials and alloys.

Aluminium alloys were the materials in scope due to their specific properties (low density and good mechanical properties) and practical applications, especially in aeronautical industries. The systematic screening and development of corrosion inhibition strategies for extensive localised corrosion conditions at selected Al alloy surfaces has been done.

To study these concepts the combination of well-known integral techniques such as EIS with sophisticated localized scanning vibrating probe technique (SVET) was systematically applied. The advantages of combining different techniques and approaches are critically analysed and evaluated from the point of view of corrosion behaviour estimation on different aluminium alloy surfaces in chloride containing electrolytic environments.

INDEX

LIST OF FIGURES

LIST OF TABLES

LIST OF ABREVIATIONS

AA2024 – 2024 Aluminium Alloy;
AA2198 – 2198 Aluminium Alloy;
μA – Micro-Ampere;
AC – Alternated Current;
BIA - Benzoimidazole;
BTA - Benzotriazole;
5Cl-BTA – 5-Chlorobenzotriazole;
CFRP - Carbon fiber reinforced polymer;
DC – Direct Current;
EIS - Electrochemical Impedance Spectroscopy;
kHz – Kilohertz;
M – Molar;
mV – millivolt;
Ω - Ohm;
ocp – Open Circuit Potential:
R_p – Polarization Resistance;
RMS – root mean square;
SVET - Scanning Vibrating Electrode Technique;
TRA – 1,2,4-Triazole;
|Z| - Magnitude of Impedance;

1. INTRODUCTION

1.1 CORROSION PROCESSES

According to NACE International's corrosion terminology, the term corrosion is defined as "the deterioration of a material (usually a metal) that results from a chemical or electrochemical reaction with its environment". [1]

Metals are usually found and extracted from nature in their oxide state (in form of compounds such as Al_2O_3, TiO_2, Fe_2O_3, etc) which is, thermodynamically their stable state. When in their elemental form (Al, Ti, Fe, etc) that stability is decreased, which means that they will force themselves to go back to their stable form – being this a thermodynamic law ("all systems tend to a state of maximum disorder"), is non-reversible.

Table 1 [2] shows the energies required to convert 1 kg of a metal from their oxide. This means that the higher the conversion energy required for this process is, the higher is the driving force that will later force the elemental form of the metal to go back to its natural state.

Table 1 - Energy required to convert oxides to produce 1 kg of their respective metal

	Metal	Oxide	Energy (MJ kg^{-1})
Highest Energy	Li	Li_2O	40.94
	Al	Al_2O_3	29.44
	Mg	MgO	23.52
	Ti	TiO_2	18.66
	Cr	Cr_2O_3	10.24
	Na	Na_2O	8.32
	Fe	Fe_2O_3	6.71
	Zn	ZnO	4.93
	K	K_2O	4.17
	Ni	NiO	3.65
	Cu	Cu_2O	1.18
	Pb	PbO	0.92
	Pt	PtO_2	0.44
	Ag	Ag_2O	0.06
Lowest Energy	Au	Au_2O_3	−0.18

Thus, when a metal is in contact with an electrolyte (aqueous solution with salts and gases dissolved in, giving water a conductively behaviour) [3] some of the ions at its surface

leave their place in the metallic matrix to go into the solution, causing the metal's dissolution under the following oxidation reaction (anodic process):

$$Metal \rightarrow Metal^{n+} + n\, e^{-} \qquad (1)$$

, where *n* is the number of electrons involved in the reaction.

If an oxidation process is occurring, a reduction (hydrogen, oxygen) process is forcibly also happening (cathodic reaction). These cathodic processes are a result of the reduction reactions given by equations (2), (3) and (4), depending on the electrochemical cell's environmental conditions such as pH and O_2 concentration.

$$2\, H^{+} + 2\, e^{-} \rightarrow H_2 \qquad (2)$$

$$O_2 + 2\, H_2O + 4\, e^{-} \rightarrow 4\, OH^{-} \qquad (3)$$

$$2\, H_2O + 2\, e^{-} \rightarrow H_2 + 2\, OH^{-} \qquad (4)$$

All these reactions can be accelerated or slowed down depending on other factors like temperature, aeration of solution (increase of O_2 concentration), amount of corrosive species in solution etc. [4]

1.2 TYPES OF CORROSION

Very often naked eye observations of metal surfaces is enough to comprise if these are being corroded although microscopic analysis is needed in some cases. This is a consequence of the different ways the above corrosion reactions can occur in these surfaces. Therefore, they can be recognised as types of corrosion. [4] A brief review on the main forms of corrosion attack is done in [2] and can be graphically represented as seen in Figure 1.

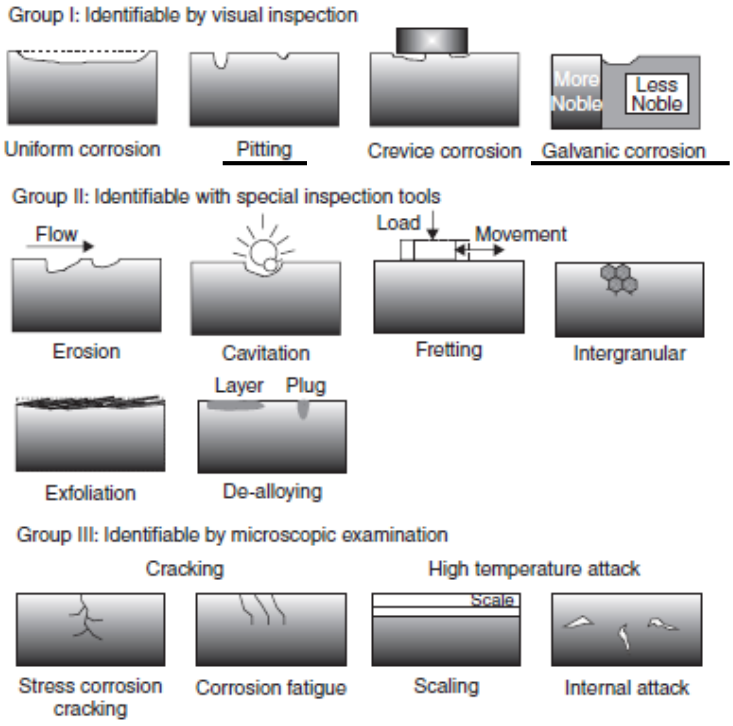

Figure 1 – Different types of corrosion grouped by means of inspection [2]

Galvanic corrosion is an electrochemical process that takes place when two different metals (materials) are connected electrically in a conductive electrolyte medium. The less noble metal (anode) will be oxidized giving electrons to the nobler one. This fact leads to dissolution of the anode element and protection of the cathode (nobler metal). So, with the help of the galvanic series table (Table 2) it is possible to join different materials and alloys without the occurrence of the corrosion phenomenon, if the chosen material are close to each in this galvanic series. If the chosen materials have a high potential difference between of them, the galvanic dissolution of the metal on the anode as well as the activity of the cathodic process will increase. [3]

On the other hand, for metals with a difference in their electrochemical potentials lower than 50mV, the probability of galvanic activity is lower.

On the **left** side of Figure 2 a galvanic couple of aluminium (Al) and Copper (Cu) is shown as well as its corrosion process, Al (the more active metal) is the metal that corrodes and Cu (nobler metal) is protected. On the **right** side of the figure it shows how a structure is affected by this type of corrosion.

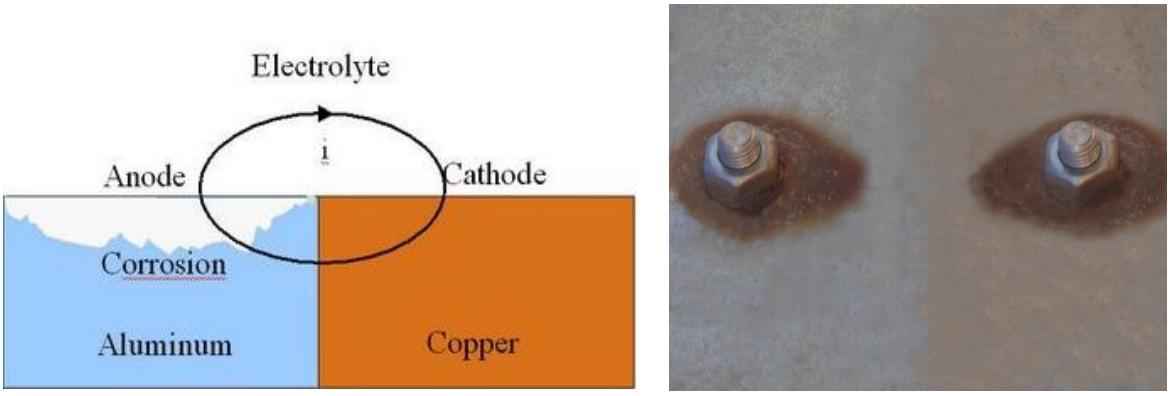

Figure 2 - Galvanic corrosion in an Al-Cu galvanic couple (**left**) and galvanically corroded structure (**right**)

Table 2 – Galvanic series of metals and alloys in seawater.

Galvanic Series of Metals and Alloys in Seawater

Active Corroded End	Magnesium	Copper
	Magnesium alloys	Aluminum bronze
	Zinc	Composition G bronze
	Beryllium	90–10 nickel
	Alchid 3S	70–30 copper-nickel; low iron
	Aluminum 3S	70–30 copper nickel; high iron
	Aluminum 61S	Nickel
	Aluminum 63S	Inconel, nickel-chromium
	Aluminum 52	alloy 600 (passive)
	Low-carbon steel	Silver
	Alloy carbon steel	Type 410 (passive)
	Cast iron	Type 430 (passive)
	Type 302, 303, 321, 347, 310, 416 (active)	Type 304 (passive)
		Type 316, (317 (passive)
	Type 430 (active)	Monel, nickel-copper
	Type 304 (active)	alloy 400
	Type 316 (active)	Hastelloy alloy C
	Ni-Resist	Titanium
	Muntz metal	Zirconium
	Hastelloy B (active)	Graphite
	Yellow brass	Gold
	Admiralty brass	Platinum
	Aluminum brass	
	Red brass	**Noble protected end**

Pitting corrosion is a localized type of corrosion that appears in small spots of the metal surface causing pits that can increase in depth until the total perforation of a metallic structure. Comparing to uniform corrosion (where the loss of material is equal in all its surface, thus visible by naked eye) the pitting can be very difficult to detect. This can be dangerous because although visual observations may report only small amounts of

corroded metal, the extent of perforation and modification of mechanical properties can lead to serious failures in the engineering systems.

A damaged oxide film or coating (scratch), the acidity or basicity of the electrolyte and the presence of differences in the metallic structure at service can also lead and influence towards higher pit propagation.

The density of pits is also an important aspect. This is related with the anodic and cathodic areas available for the oxidation and reduction reaction to occur. Equation (5) shows that the higher the cathodic/anodic area ratio is, the higher is the anodic current density and therefore more serious is also the pit propagation (corrosion) [4].

$$I_a = I_c \rightarrow i_a * S_a = i_c * S_c \rightarrow i_a = i_c * S_c / S_a \qquad (5)$$

, where I_a and I_c are the anodic and cathodic currents, i_a and i_c are their current densities and S_a an S_c the anodic and cathodic areas, respectively.

1.3 PREVENTIVE METHODS

Despite the non-reversible character of the corrosion phenomenon there are ways of preventing and mitigating it. This means that for a different type of corrosion occurrences there are different approaches that can be used in order to stop the corrosion.

The mitigation of **pitting corrosion** can be achieved by the coating of the metal surfaces, for example by painting it. This layer will prevent the corrosive species to contact with the metal's surface thus providing the necessary barrier protection. Another approach is the use of inhibitors that can be added to the coating or to the environment itself (electrolytic solution). This addition will alter the electrode reactions of the cell hence removing the driving force for them to occur. [2]

In the case of **galvanic corrosion**, the protection can be achieved by taking into account the following factors:

- Avoid constructions with connections between dissimilar metals. The bigger the difference on the electrochemical potentials between the metals in this table, the higher the tendency for the more active one to corrode when connected to the other. In the opposite way, materials close in this table are less likely to provoke corrosion in the more active one.
- The use of insulating materials between the metals interfaces (the connection between the metals is then vanished and they will both solely corrode with no interference of the other).

- Supress anodic and/or cathodic activity – if the cathodic activity is suppressed then forcibly the anodic reaction stops as well.

In the present work, all the focus was given to the cases of pitting and micro-galvanic corrosion since these are 2 of the most common types of corrosion that tend to occur on bare surfaces of AA due to specific properties of these alloys.

The main idea was to systematically track which were the inhibitors that presented better corrosion protection of these alloys when added to a selected corrosive medium.

The use and combination of integral and localized electrochemical techniques as well as the correlation between collected results allows to understand and conclude in the end which are, from all inhibitors tested, the ones more suitable for corrosion protection of the selected alloys.

Deeper explanations on these matters (difference between alloys, how the used inhibitors act, etc.) will be given in the following sections of the present work.

1.4 ALUMINIUM ALLOYS

These alloys usually present relatively low values of density, high conductivities (thermal and electrical) and satisfying corrosion resistance [11], depending on the environment they are put in. The alloying of aluminium is done in order to improve the mechanical strength of the material, but it leads to the appearance of intermetallic phases in the alloys matrix a factor that has effects on its corrosion resistance, tendentiously lowering it [6, 8, 9]. Aluminium alloys can be cast or wrought and can be alloyed with various elements and the most common alloying elements are copper (Cu), zinc (Zn), magnesium (Mg), silicon (Si) and manganese (Mn). These differences lead to distinct properties of the final alloys and these differences in the properties and type of alloys divides them into families or series. The series of Al alloys range, commonly, from 1xxx to 8xxx [5].

In the frame of this work the 2xxx family is considered and this series of alloys is widely used in different industrial areas, such as automotive and aircraft industries.

1.4.1 AA2024

AA2024 is widely used in aeronautical industries due to its good strength to weight ratio. As seen above, the problem of alloying aluminium with other elements is that although its strength/ratio can be improved, it probably will lower the corrosion resistance of these

alloys. In the case of AA2024 the copper is the major alloying element as it can be seen Table 3 [6].

Table 3 - Chemical composition of AA2024-T3

Elements	Cu	Cr	Si	Fe	Mg	Mn	Ti	Zn	other	Al
%wt	3.8-4.9	0.1	0.5	0.5	1.2-1.8	0.3-0.9	0.15	0.25	0.15	Balance

The two major alloying elements in this type of alloy are copper and magnesium and the presence of these species will create significant amounts of intermetallic phases with the compositions Al_2CuMg and lower amount of other intermetallic phases due to the presence of other species in lower quantities as alloying elements [6, 8]. These intermetallic phases, specifically Al_2CuMg, will behave as localized anodes and cathodes simultaneously in the electrochemical environment when compared to the alloy's matrix. This is due to the presence of copper, which is a nobler material when compared to aluminium and magnesium in the opposite side, thus creating localised micro-galvanic systems on the metal's surface. Since these phases are present in small areas of the alloy's surface, this will tendentiously lead to the corrosion occurrence in localized spots of the surface, which leads to pitting form of corrosion. [6, 9]

1.4.2 AA2198

AA2198 is a lithium containing aluminium alloy and its chemical composition is given in Table 4 [10].

Table 4 - Chemical composition of AA2198

Elements	Cu	Li	Si	Fe	Mg		Mn	Ti	Zr	Zn	Al
%wt	3.68	1.01	0.03	0.08	0.31		-	0.0027	0.12	0.01	Balance

The inclusion of lithium in the chemical composition of this type of alloy helps to achieve analogous values of mechanical strength when compared to other alloys from the 2000 series, with the benefit of the final weight of the alloys being slightly lower (mass reduction). Also, AA2198 contains lower quantity of copper, which decreases the tendency for the corrosion occurrence due to the smaller amount of strong cathodic intermetallic phases. These characteristics make this type of alloys very interesting for various industrial areas, such as aeronautical industries. It will be later be shown in the experimental results

that as it could be expected this alloy shows slightly lower corrosion activities when compared to AA2024. [10, 11]

1.5 INHIBITORS

One general way to supress the corrosion phenomena is the usage of different corrosion inhibitors and these can be classified as organic and inorganic.

1.5.1 ORGANIC INHIBITORS

Organic inhibitors work against the corrosion processes due to their capacity to form protective adsorption or complex adlayers on metallic materials which helps to decrease the anodic and cathodic activities thus blocking the corrosion process

During the present work different azole derivatives as organic inhibitors were chosen such as: 1,2,4-Triazole (TRA), Benzoimidazole (BIA), Benzotriazole (BTA) and 5-Chlorobenzotriazole (5Cl-BTA) and this selection was done based on previous studies done with this type of inhibitors [9, 12] where it is stated that they can efficiently act on the suppression of corrosion activities due to their tendency to adsorb onto copper particles which are significantly present in the studied alloys.

1.5.2 INORGANIC INHIBITORS

Salts of rare earth elements are an example of inorganic inhibitors and their main role is to form highly insoluble deposits on the cathodic intermetallic areas. This protection is achieved because the precipitation of the formed hydroxides ($Ln(OH)_3$, where Ln is the rare earth metal element) will block the cathodic reactions on the surface. [6, 13].

In the sense of this work the selected inorganic inhibitors were Cerium (III) and Lanthanum (III) Nitrate, since they tend to show good inhibitive properties for AA2024 [6, 13] which can be also taken into account for the case of AA2198.

1.5.3 INHIBITORS COMBINATIONS

Previous studies [13, 14, 15] have shown that combining different inhibitors with different inhibition mechanisms can increase their effectiveness compared to them standing alone. In that sense, different combinations were studied and they are: BTA + Cerium (III) Nitrate, 5Cl-BTA + Cerium (III) Nitrate and 5Cl-BTA + Lanthanum Nitrate.

2. ELECTROCHEMICAL TECHNIQUES

2.1 SCANNING VIBRATING ELECTRODE TECHNIQUE (SVET)

SVET measures potential differences in solution caused by ionic fluxes that arise from electrochemical reactions occurring in the corroding metal surface. A calibration converts the measured potential differences in solution into the ionic currents [16, 17] and can be suitably applied for monitoring of galvanic and microgalvanic corrosion [13]. This technique enables the calculation of the current density (i), using the values of potential difference (ΔV) between two points in solution. These measured positions are separated with a determined distance (Δr). The current density is calculated with the use of the following equation,

$$i = \kappa^* E = - \kappa * \Delta V / \Delta r \qquad (6)$$

where κ is the solution's conductivity, E is the solution's electrical field and ΔV is the potential difference between the positions in solution at a distance Δr. The use of a vibrating electrode is an advantage of this technique because it helps to lower the noise in the measurements and increase the sensitivity. One of the disadvantages of this method is that although it can be used to estimate corrosion rates, the estimated values are associated to high values of uncertainty [15] because the measurements are typically done close to (100 – 200 µm), but not completely on the metals surfaces.

A typical current density map for zinc (Zn) – iron (Fe) galvanic couple measured by SVET is given in Figure 3, and the occurring electrochemical processes of this couple is given in Figure 4 [18].

It can be seen that in the case of this galvanic couple, that the more active metal (anode) is Zn and the nobler one is Fe. The current densities on the anode will show higher values than those measured above the cathodes.

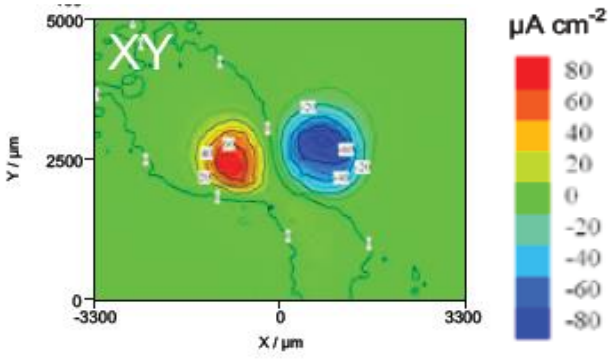

Figure 3 - SVET measurement of current density map of Zn – Fe galvanic couple

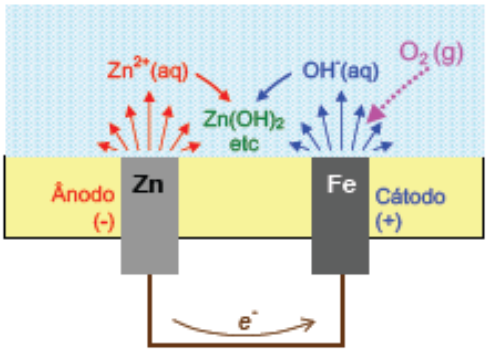

Figure 4 - Zn – Fe galvanic couple and occurring electrochemical processes

2.2 ELECTROCHEMICAL IMPEDANCE SPRECTROSCOPY (EIS)

With EIS technique it is possible to understand the kinetic characteristics of electrochemical systems, from rate constants to diffusion coefficients [19]. The basis of this method is the appliance of a potential difference to an electrochemical system and the measuring of the resulting current through the system. EIS is usually measured using a small excitation signal. If there is a linear (or pseudo-linear) system, the current response to a sinusoidal potential excitation will come as sinusoid, with the same values of frequency, but with a phase shift (Figure 5)

.

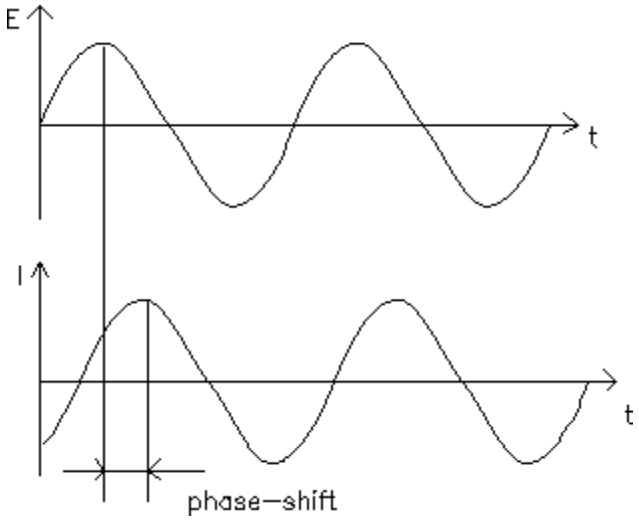

Figure 5 - Sinusoidal response of the system to an applied sinusoidal excitation

The excitation signal (as a function of time) comes as

$$E_t = E_0 \sin(\omega t) \qquad (7)$$

, where E_t is the potential at a time t, E_0 is the amplitude of the signal and ω is the radial frequency.

In a linear system, the response signal, I_t, is shifted in phase, φ, with different amplitude than I_0.

$$I_t = I_0 \sin(\omega t + \varphi) \qquad (8)$$

Taking Ohm's law into consideration, an expression analogue to that can be used to calculate the impedance of the system

$$\boldsymbol{Z} = E_t / I_t = E_0 \sin(\omega t) / I_0 \sin(\omega t + \varphi) = \boldsymbol{Z_0 * \sin(\omega t) / \sin(\omega t + \varphi)} \qquad (9)$$

In this type of measurements usually the impedance is represented as a complex number, with the help of Eulers relationship

$$\exp(j\varphi) = \cos\varphi + j.\sin\varphi \qquad (10)$$

and the values of impedance will come after the following equation

$$\boldsymbol{Z(\omega)} = E / I = Z_0 \exp(j\varphi) = \boldsymbol{Z_0 (\cos\varphi + j.\sin\varphi)} \qquad (11)$$

Using this equation and plotting the imaginary part of the equation as a function of the real part, leads to a Nyquist Plot. Each point in this plot is the impedance at one frequency.

The impedance |Z| is then a vector sum of imaginary and real part, as it can be seen in Figure 6. It is important to notice that Figure 6 only shows one type of response for a given signal and that response is particular from the material. If the measurements were done in an electrochemical cell with several different properties than the other, the response signal will have different shapes.

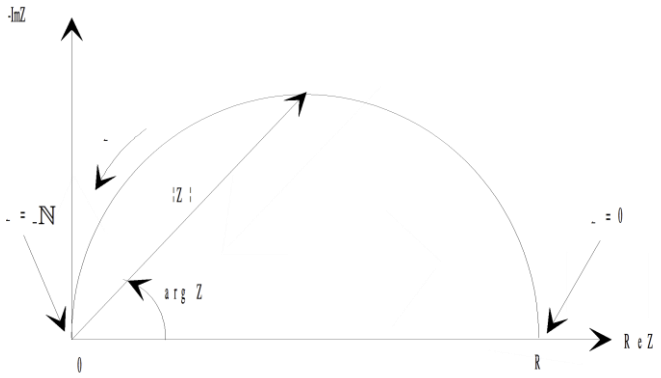

Figure 6 - Nyquist Plot of an electrochemical system

The major problem of a Nyquist Plot is that it is not possible, when taking a look at any point of the plot, to read the frequency used to record that point. One way to overcome this limitation is to use the impedance data and plot the systems' total impedance values |Z| and phase angle (theta) against frequency. These are called Bode plots and an example can be seen in Figure 7.

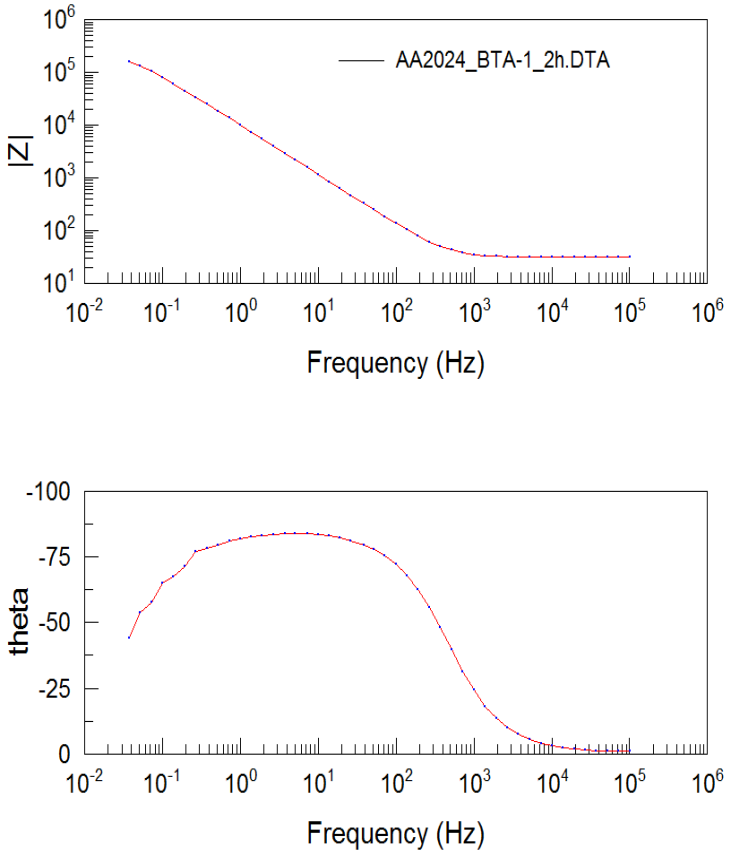

Figure 7- Bode Plot of an electrochemical system

3. EXPERIMENTAL DETAILS

3.1 SAMPLE PREPARATION

The bare polished surfaces of AA2024 and AA2198 were the selected substrates for all experiments. In order to guarantee a good reproducibility of the results and systematic approach the special attention has been paid to the relevance of routine sample preparation.

3.1.1 SVET SAMPLES

SVET samples were prepared from given flat sheets of both alloys of approximately 6mm of thickness. These were cut into small pieces of 6*6mm and 4 mm thickness. The desired shape was achieved by careful polishing. The alloys were polished following a gradually decreasing grain size polishing paper: from P320 to P600, P800 and then P2500 in order to obtain mirror-like surfaces of the alloys. This was necessary in order to obtain clean and reproducible surfaces of the alloys.

The next step and one of the most important part was the side isolation of these samples before casting them into epoxy resin. This was done in order to seal the interfaces between the sample and resin, thus preventing the corrosive solutions to get into these gaps, which would lead to localized and centres for crevice corrosion to occur. Figure 8 shows two SVET maps after of AA2024 after 2 hours of immersion in 0.05M NaCl, which was resulting with extensive corrosion activities on the edges of the electrode **(a)** and a uniformly corroding sample isolated with Bees wax in 0.05M NaCl, respectively. Figure 8(a) shows that all activities are concentrated near the sides of the sample and it does not allow the adequate assessment of activities, which does not happen in the case of a Bees wax isolated sample. Equally with Bees wax also the high grade Apiezon wax has been also successfully implemented for the same purpose. The final developed SVET sampling system (sample + epoxy resin) is shown in Figure 9. On the **left**, the whole system in normal size and on the **right**, the system at its measuring state (enlarged) with the blue dashed line representing SVET surface mapping the area.

(a)

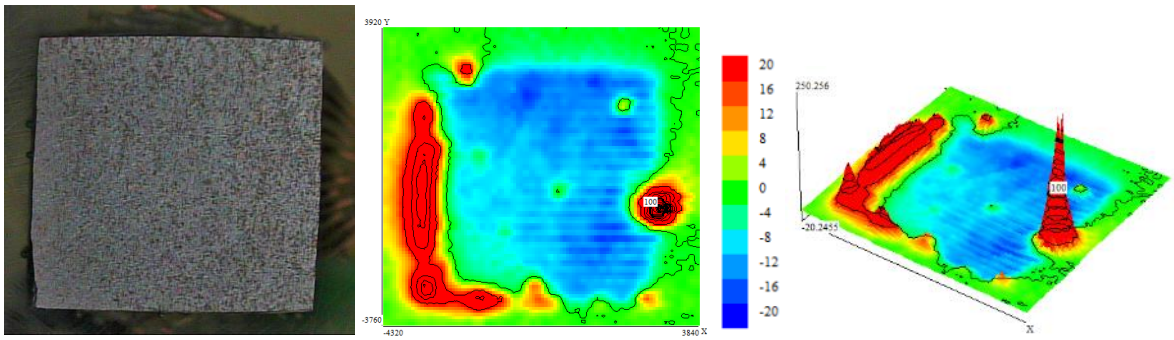

(b)

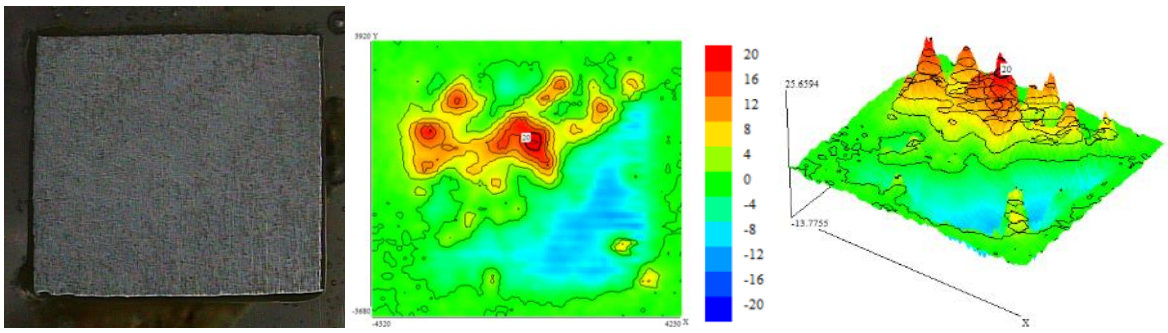

Figure 8 - AA2024 immersed for 2 hours in 0.05M NaCl - **(a)** non-isolated and **(b)** Bees wax isolated

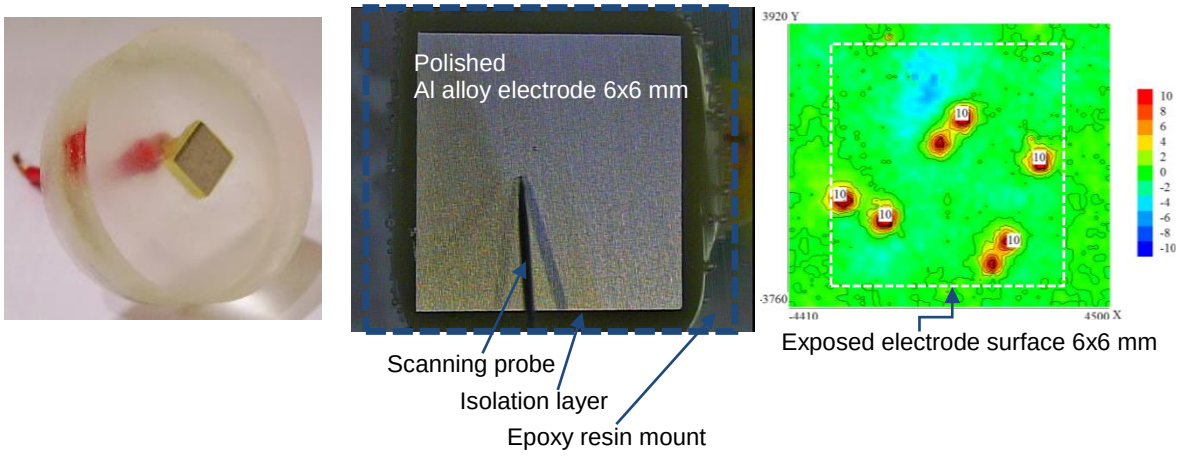

Figure 9 – Electrodes for SVET in cast-epoxy mount and SVET map.

3.1.2 EIS SAMPLES

EIS samples were prepared from the same aluminium alloy sheets as those prepared for SVET measurements. In this case, the sheets were cut into relatively bigger pieces (around 30*30mm), but with the same thickness and polished in the same way as SVET electrodes. After this, pieces of plastic tubes (solution containers) were glued onto the sample's surfaces with commercially available araldite epoxy resin. Once the containers

were attached to the alloys the exposed area for corrosion tests was 3.35cm^2 and with only few cases by technical reasons of 2cm^2. For data treatment and analysis all EIS data was normalized to 1cm^2.

Figure 10 shows a sample of AA2198 for EIS experiment. On the **left**, the sampling system in solution with immersed Pt-wire counter and saturated calomel reference electrode. And on the **right** the top-photograph for the sample after one day of immersion in 0.05M NaCl.

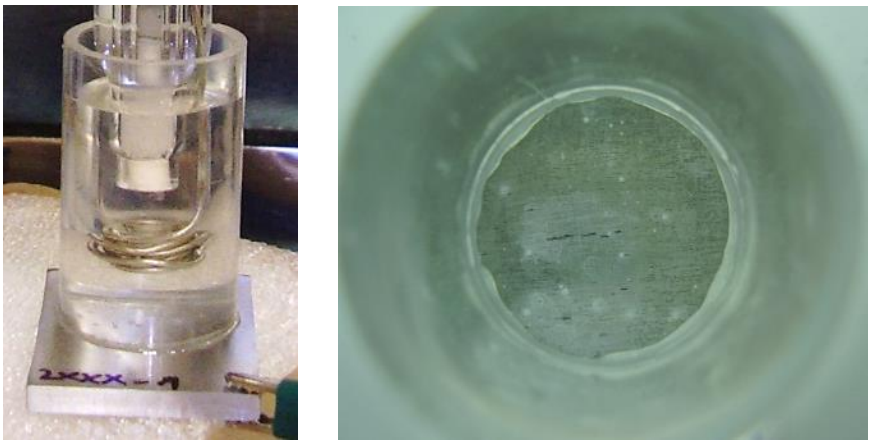

Figure 10 – EIS sampling systems seen from side and top view, respectively.

3.2 SOLUTION PREPARATION

To carry out this work a number of inhibitor solutions were prepared in 0.05M NaCl supporting electrolyte (reference corrosive media) solution. The following table is used to show all the selected inhibitor solutions and inhibitor combinations used throughout the experiments carried out during this Master Thesis. All the solutions presented on Table 5 were prepared from commercially available nearly pure chemicals (Sigma-Aldrich), weighted with analytical grade balance and dissolved in deionized (R: 18.2 MΩ.cm) water.

Table 5 – Inhibitor solutions added to the reference solution of 0.05M NaCl before dilutions.

Single Inhibitors	Inhibitor Combinations
5mM 5Cl-BTA	5mM [5Cl-BTA + Cerium (III) Nitrate]
5mM BIA	
5mM BTA	5mM [5Cl-BTA + Lanthanum (III) Nitrate]
5mM 1,2,4-Triazole	
5mM Cerium (III) Nitrate	2.5mM [BTA + Cerium (III) Nitrate]
5mM Lanthanum (III) Nitrate	

Later in this work a second study was done in order to understand the effect of the inhibitors concentrations on their corrosion protection behaviour and for such matter some variations of three of the presented systems were prepared by dilution.

These three chosen solutions presented on Table 5 were ***5mM 5Cl-BTA***, ***5mM [5Cl-BTA + Cerium (III) Nitrate]*** and ***5mM [5Cl-BTA + Lanthanum (III) Nitrate]***. Dilutions of 10, 100 and 1000 times were done in order to fit the concentrations of 0.5, 0.05 and 0.005mM in 0.05M NaCl supporting electrolyte for all three different inhibitor systems.

3.3 TESTING METHODOLOGIES

3.3.1 SCANNING VIBRATING ELECTRODE TECHNIQUE - SVET

For SVET measurements commercial measurement system from Applicable Electronics Inc. (USA) controlled by the ASET 2.0 software from ScienceWares Inc. (USA) has been used (Figure11). The microelectrodes were Pt–Ir wires from MicroProbes Inc. (USA) with insulated shaft and a platinum black deposit on the tip with up to 10 μm in diameter. The probe was located 200 μm above the surface and vibrated in the Z direction (normal to the surface) with frequency of 398 Hz and amplitude of 10 μm. For different purposes, the software allows to configure and vary selected variables of measurement such as the distance between the vibrating electrode and the sample surface, the number of points measured in a specific area, the interval time between scans and the number of scans to be done, etc.

This technique allows to know and monitor the local ionic currents (fluxes) in active metallic surfaces immersed in an electrolyte medium. SVET is a non-invasive technique that allows detecting anodic (positive currents) and cathodic (negative currents) zones above the corroding surface immersed in aggressive media [17].

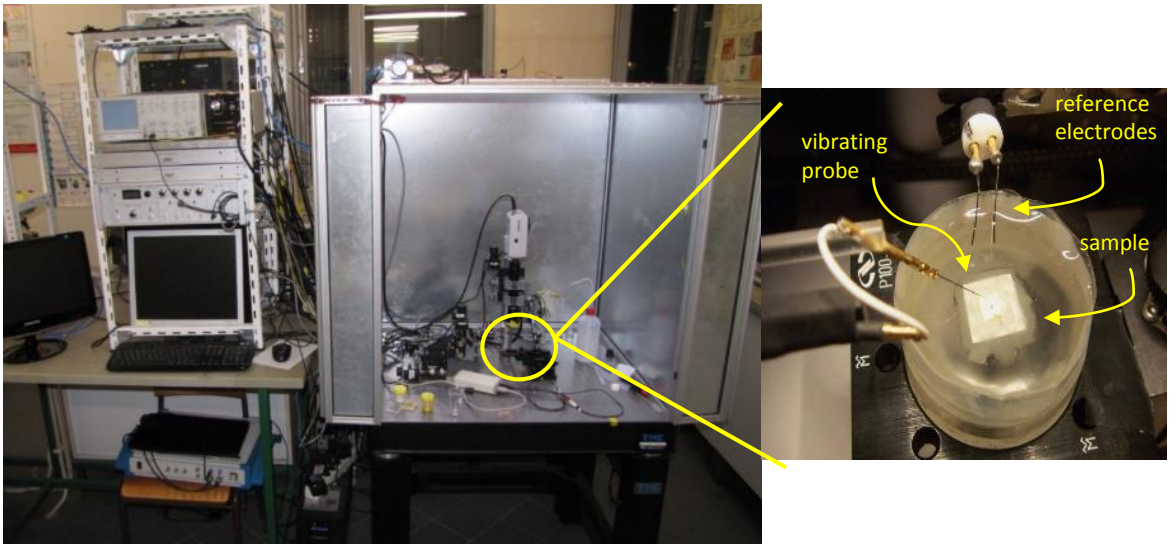

Figure 11 – Faraday cage connected to a PC with ASET software (**left**) and magnification of the sample holder inside the cage (**right**)

3.3.2 ELECTROCHEMICAL IMPEDANCE SPECTROSCOPY - EIS

The EIS test system used was Reference 600 (Gamry, USA) and the experimental set up can be seen in Figure 12. On the **left** of the figure the whole system is mounted and connected to the potentiostat. The potentiostat by itself is connected to a PC where data can be recorded and evaluated with Gamry's software. On the **right** of the figure, the testing system is magnified (bare surface of AA immersed in corrosive/inhibitive solution) and connected to a 3 electrode testing system containing of working electrode (aluminium alloy), reference electrode (saturated calomel) and counter electrode (Pt wire).

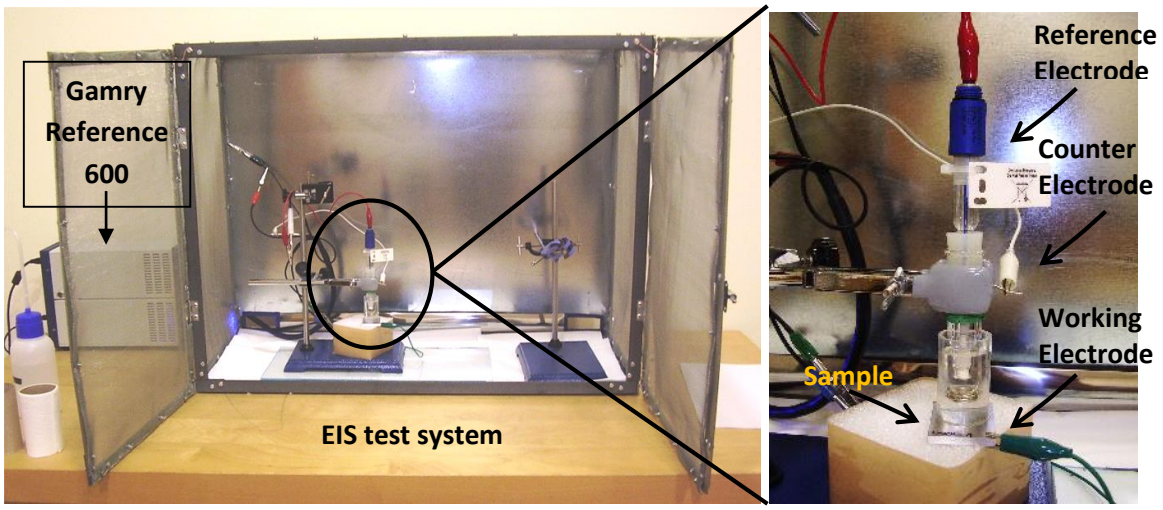

Figure 12 – Gamry Reference 600 test system (**left**) and measurement set up (**right**)

All measurements were done at open circuit potential applying 10mV sinusoidal perturbation (RMS) in the 100 kHz to 10 mHz frequency range. Seven experimental points per frequency decade were usually collected during the measurements.

4. RESULTS AND DISCUSSION

4.1 STUDY OF INHIBITOR SYSTEMS

4.1.1 EIS

The systematic EIS analyse was done for all inhibitor systems listed in Table 3, for the following times of immersion: 0 hours (~20 minutes), 2 hours, 4 hours, 1 day, 2 days, 1 week, 3 week and 2 months. Only in case of more actively corroding systems the longer immersion times (3 weeks and 2 months) because the samples were already highly corroded.

This section pretends to show the effect of selected corrosion inhibitors to the aluminium alloys substrate, when added to the base corrosive media - reference solution (0.05M NaCl). Total impedance (|Z| / $\Omega.cm^2$) at selected relevant frequency and fitted polarization resistance (R_p) were the main parameters used for corrosion activity assessment on all studied systems. Figure 13 shows the two equivalent circuits used for all the fittings. The one in the **left** used for systems presenting only one time constant in the spectra and in the **right** for systems presenting two time constants:

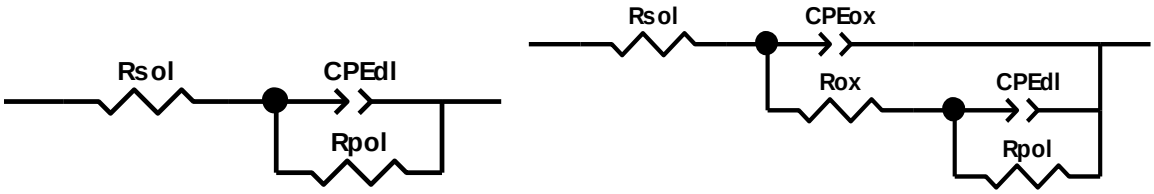

Figure 13 – Equivalent circuits used for EIS spectrum study – one time constant (left) and two time constants (right)

, where R_{sol} is the solution's resistance, CPE_{dl} is the Constant Phase Element associated to a double layer capacitor present on the metal's surface and R_{pol} is the Polarization Resistance. In the case of the two time constant circuit, the values CPE_{ox} and R_{ox} appear due to the degradation of aluminium oxide layer (this tends to happen for longer immersion times, but in those highly corroding systems it is visible rather earlier) and are the Constant Phase Element and the Resistance associated to that oxide layer.

The evolution of the |Z| for AA2024 and AA2198 immersed in 4 different solutions are presented in Figures 14 and 15 respectively. The different shapes of spectra can be observed suitable for modelling with 1 on 2 time constant equivalent circuits. Also all selected inhibitor systems show clearly the effect to the observed impedance values indicating to efficient protection properties.

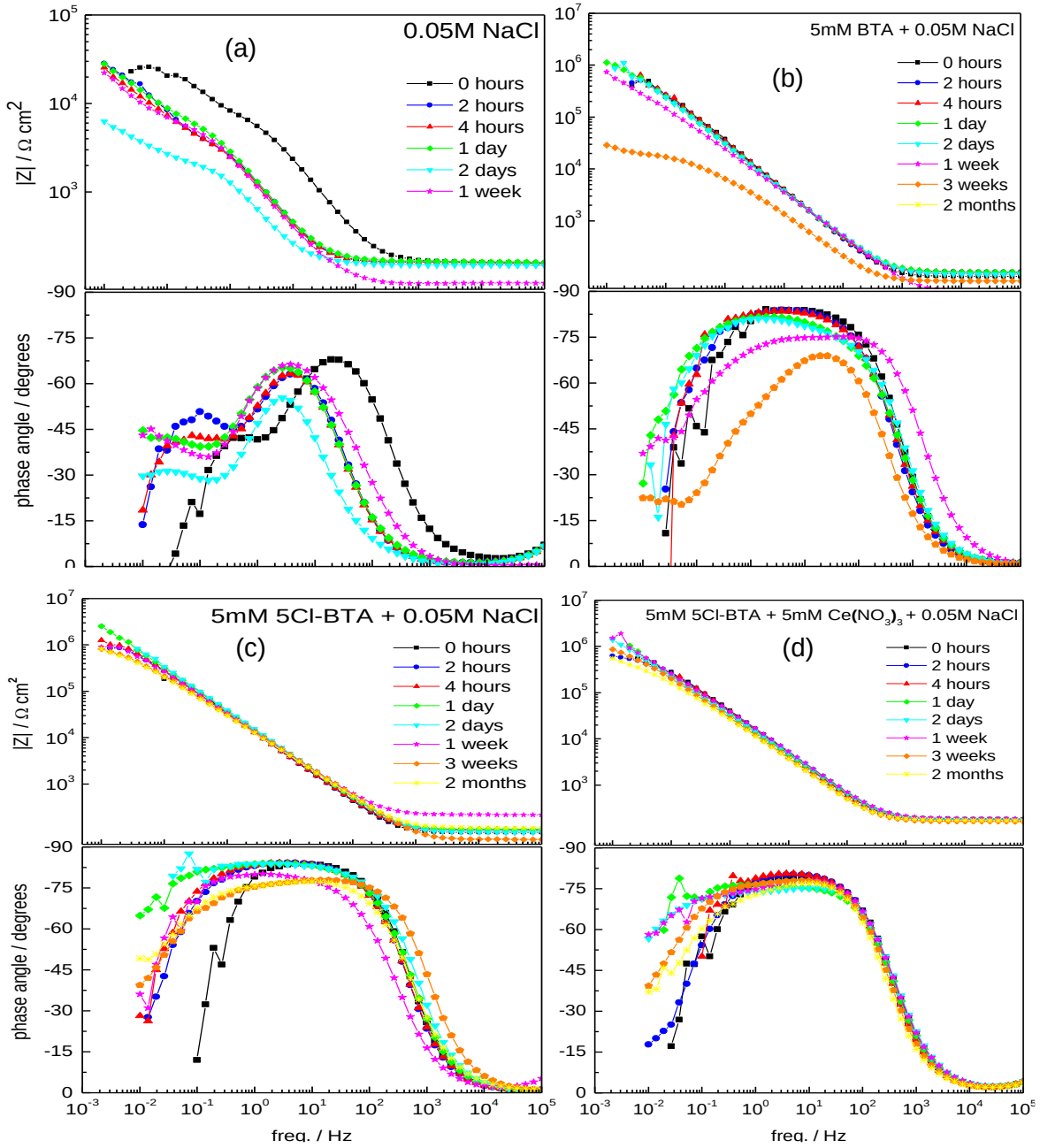

Figure 14 – Bode plots for AA2024 immersed in (a) NaCl reference solution and with addition of (b) BTA, (c) 5Cl-BTA and (d) combination of inhibitors (5Cl-BTA + Cerium (III) Nitrate).

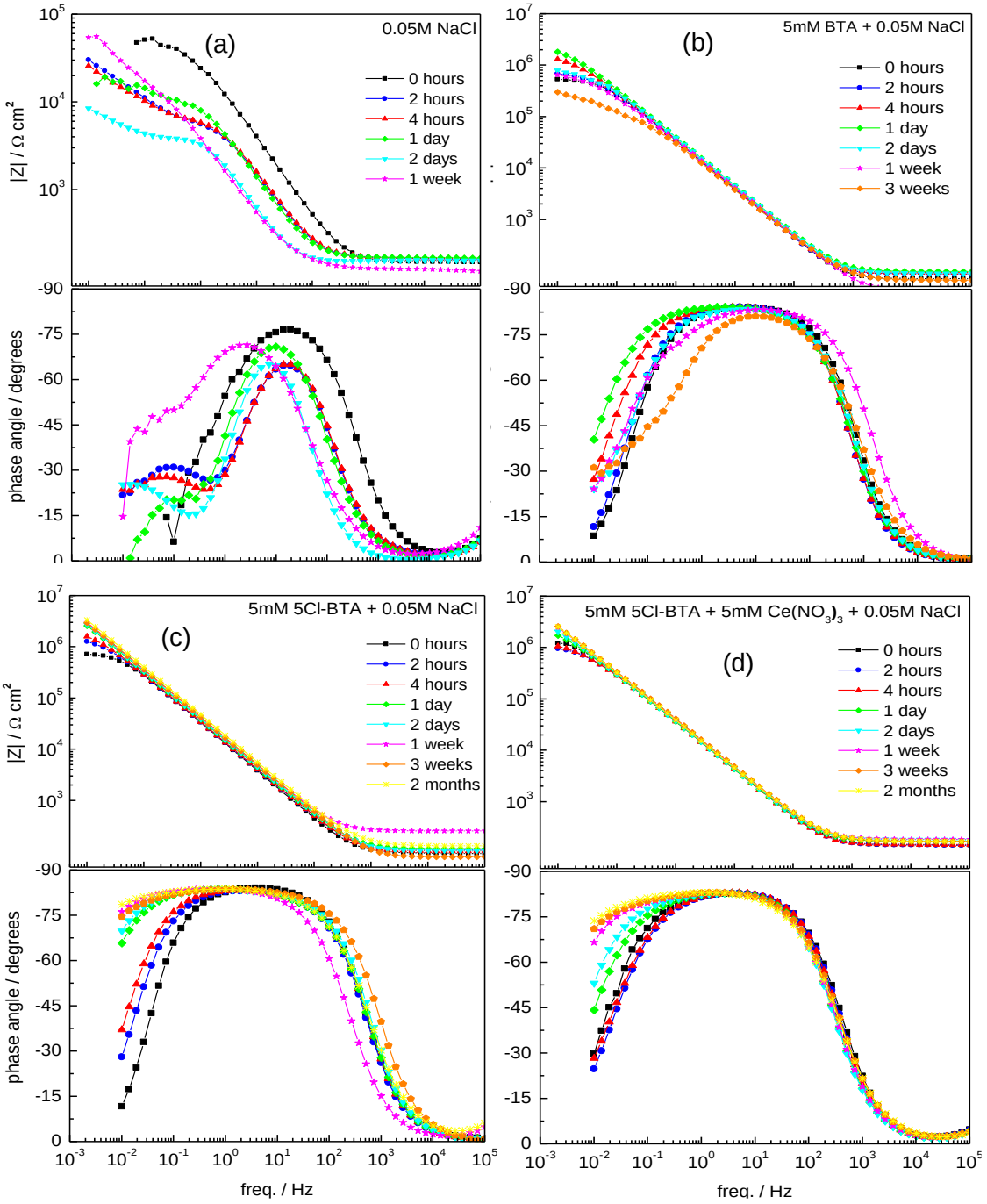

Figure 15 – Bode plots for AA2198 immersed in (a) NaCl reference solution and with addition of (b) BTA, (c) 5Cl-BTA and (d) combination of inhibitors (5Cl-BTA + Cerium (III) Nitrate).

In order to show the Bode plots at selected immersion times for all tested inhibitor systems the Figures 16 and 17 for AA2024 and AA2198 are respectively presented. The chosen immersion times were: 4 hours, 2 days, 1 week and 3 weeks. Also the photos related to the immersed alloys in some of those different inhibitor systems at selected immersion times are shown in Table 7.

Table 6 – AA2024 and 2198 immersed in different inhibitor systems at selected times

Inhibitor System	AA2024		AA2198	
Reference	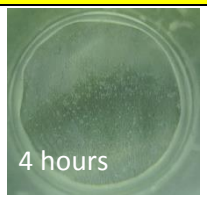		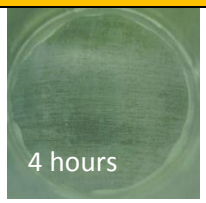	
BTA	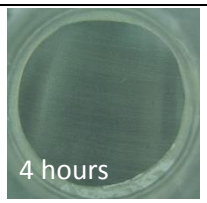	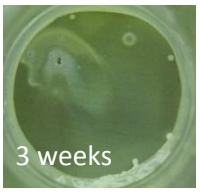	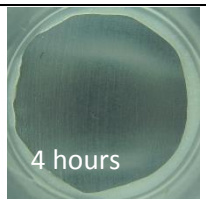	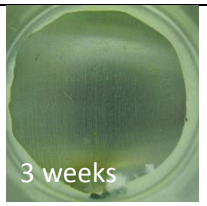
BIA	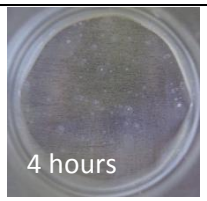		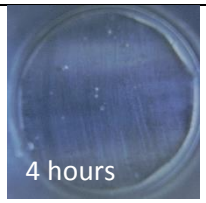	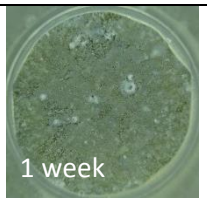
5Cl-BTA	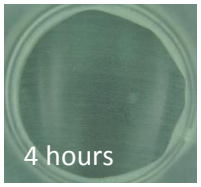	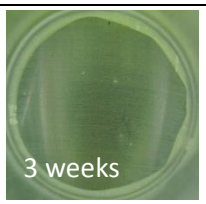	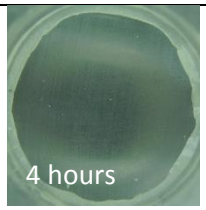	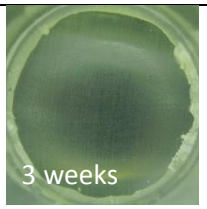
Ce^{3+}	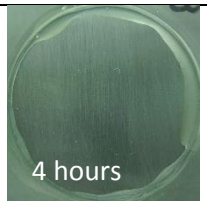		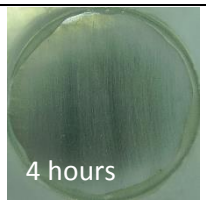	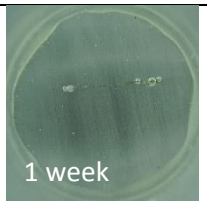
BTA + Ce^{3+}		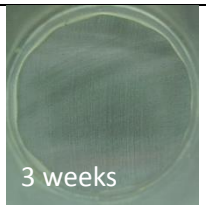	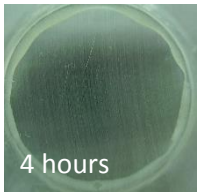	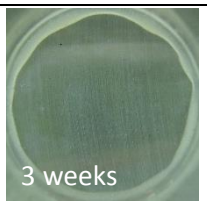
5Cl-BTA + La^{3+}	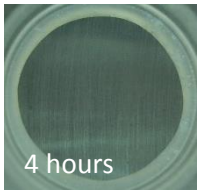	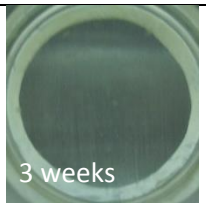	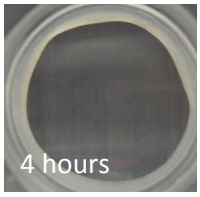	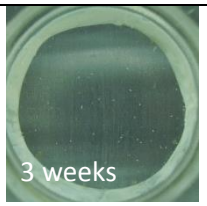

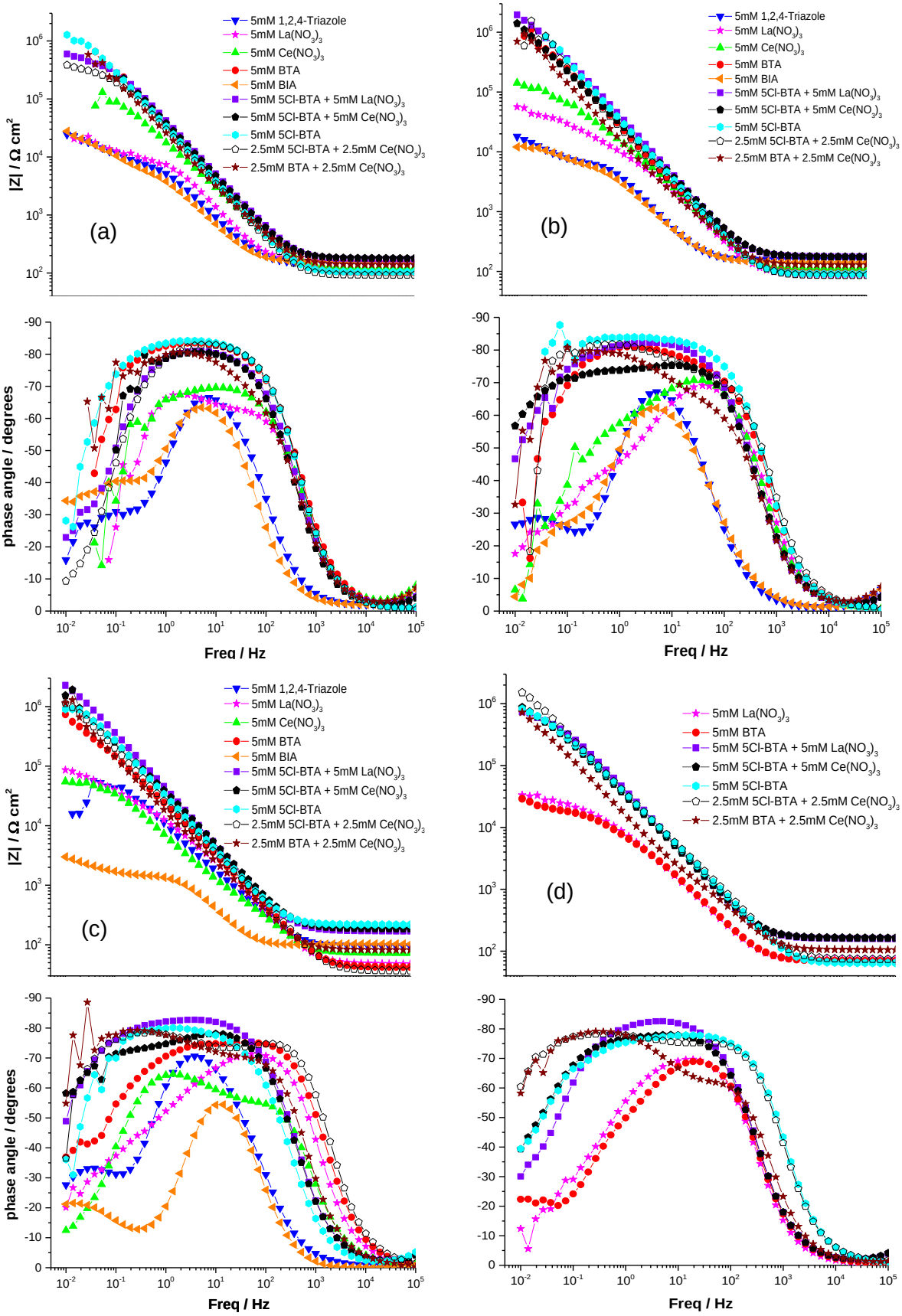

Figure 16 - Bode plots for AA2024 immersed in all inhibitor systems for (a) 4 hours, (b) 2 days, (c) 1 week and (d) 3 weeks.

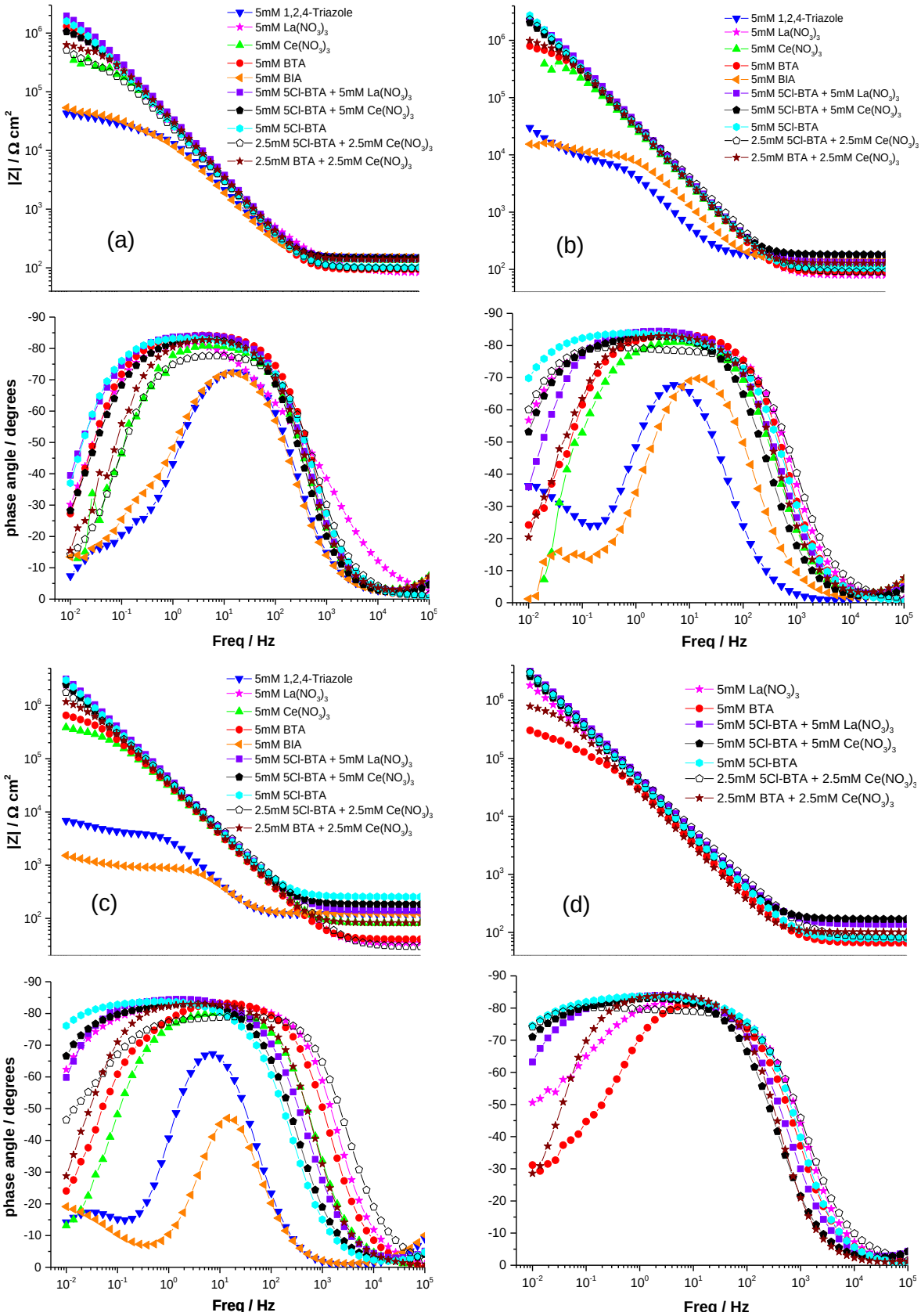

Figure 17 - Bode plots for AA2198 immersed in all inhibitor systems for **(a)** 4 hours, **(b)** 2 days, **(c)** 1 week and **(d)** 3 weeks.

This second type of data presentation promptly shows how the systems behaviour during the time and generally distinguishes the efficiencies of tested inhibitors.

The overall EIS results show completely non inhibitive properties of 1,2,4-Triazole and BIA on both alloys as the impedance |Z| decreases very rapidly with time – showing values of 2 and 3 orders of magnitude lower when compared to the other systems.

For an overall and better understanding of corrosion activity of these systems, the Low Frequency |Z| at certain frequency (0.1Hz) has been plotted versus immersion time. Figures 18 and 19 show this evolution for AA2024 and AA2198 respectively (the single inhibitor systems and combination inhibitor systems are presented in different plots).

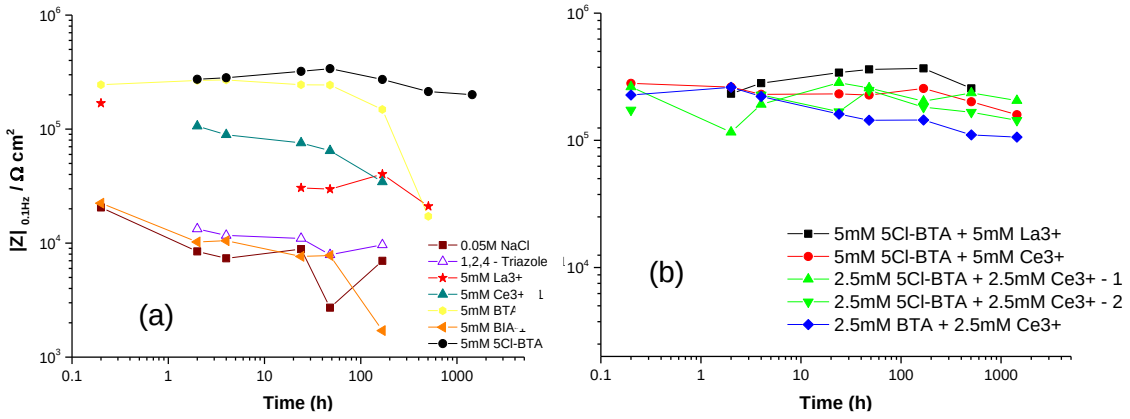

Figure 18 - Evolution of low frequency impedance |Z| (0.1Hz) vs. time (h) for **(a)** all inhibitors and **(b)** inhibitor combination systems for AA2024.

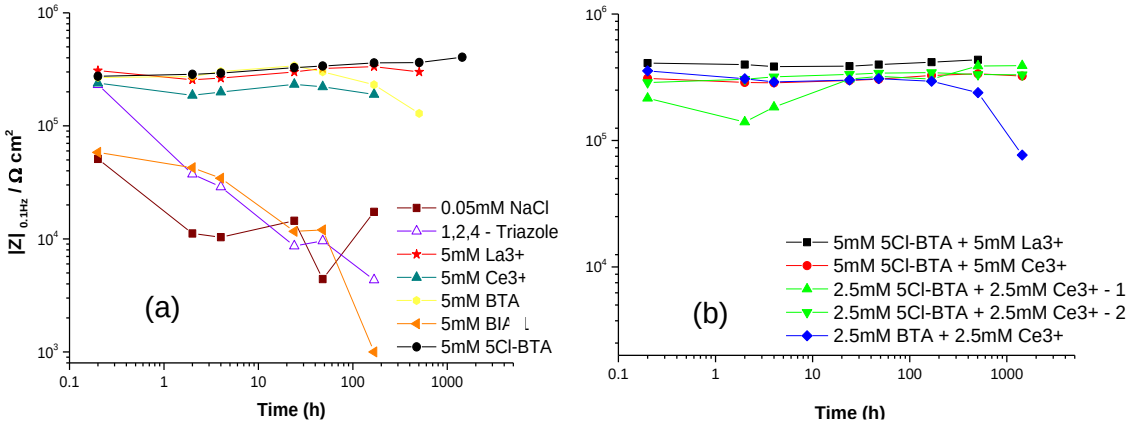

Figure 19 - Evolution of low frequency impedance |Z| (0.1Hz) vs. time (h) for **(a)** all inhibitors and **(b)** inhibitor combination systems for AA2198.

It can be seen in Figures 18 and 19 that only 5Cl-BTA (as a single inhibitor) presents good inhibitive behaviour for both alloys in case of longer immersion period. In all other mediums the protective properties were lost after 1 week. However, especially in the case of AA2198 immersed in Lanthanum (III) Nitrate the low frequency impedance keeps still

being amongst the best protective systems. Also all combination inhibitor systems, excluding BTA + Cerium (III) Nitrate, present good inhibitive behaviour for long immersion period.

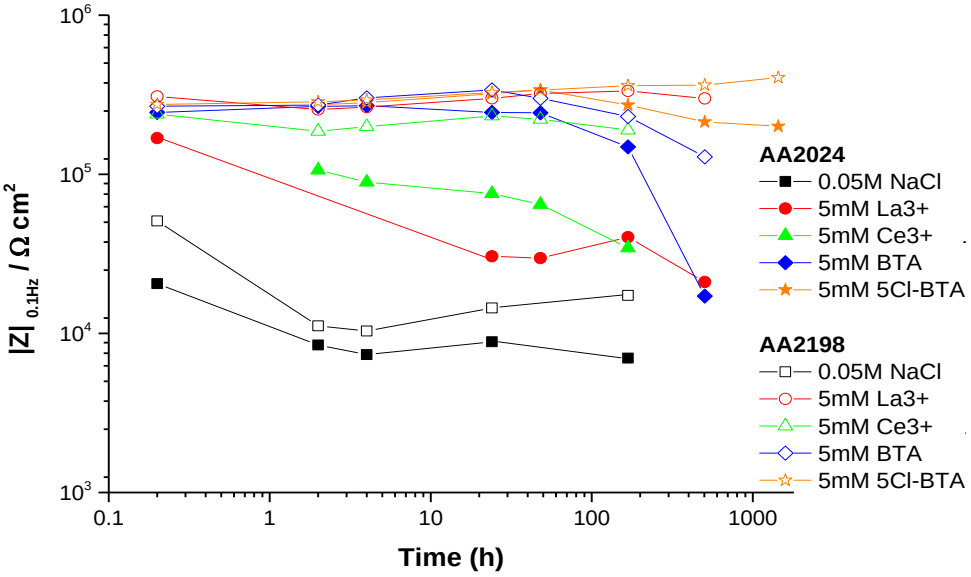

Figure 20 - Evolution of low frequency impedance |Z| (0.1Hz) vs. time (h) for both alloys with selected single inhibitors.

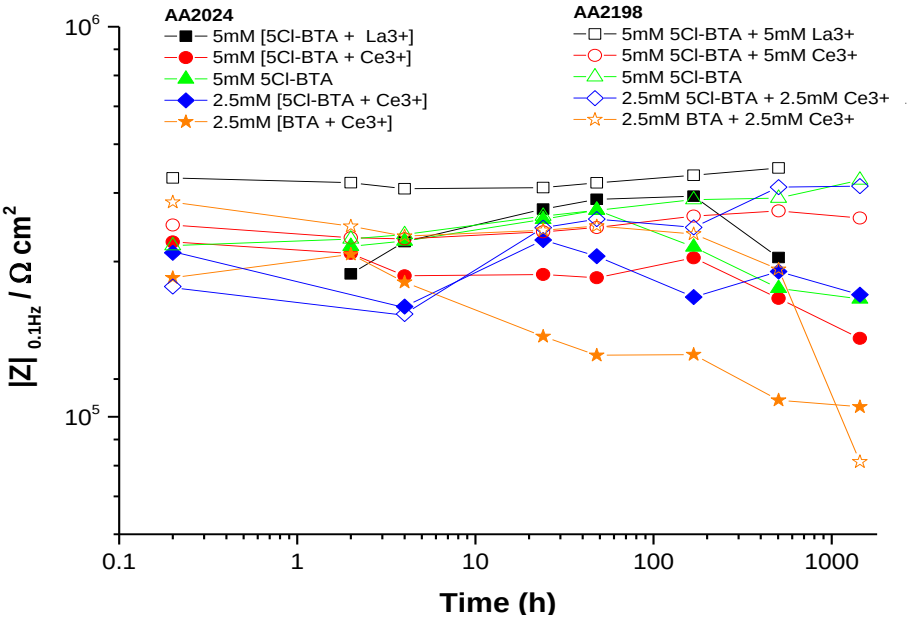

Figure 21 - Evolution of low frequency impedance |Z| (0.1Hz) vs. time (h) for both alloys with 5Cl-BTA and 3 selected inhibitor combinations.

Figures 20 and 21 show that in the case of these selected better performing inhibitor systems (single or combination) the plotted low frequency impedance (|Z| at 0.1Hz) values

are generally higher in the case of AA2198. This means that the inhibition efficiencies for most of the inhibitor systems are somewhat better in the case of AA2198 than AA2024. It can be related with the distribution and composition of intermetallic phases in the alloy matrix. AA2198 has Li instead of Mg and significantly lower concentration of Cu (when compared with AA2024), which apparently decreases the occurrence of localised micro-galvanic activities significantly.

In order to estimate more precisely the corrosion properties the obtained EIS spectrums were fitted in order to estimate the Polarization resistances for these systems. The Polarization resistances will then later be used in order to quantify the efficiency of all tested inhibitors and inhibitor combinations. The used Equivalent Circuits are presented above in Figure 13. As a result of these fittings, the R_p values vs. time for all inhibitor systems and inhibitor systems combinations obtained are presented in Figures 22 and 23 for AA2024 and AA2198 respectively. After this the alloys and inhibitor systems were compared to each other similarly like previous data discussion of Low frequency |Z| vs time – Figures 24 and 25.

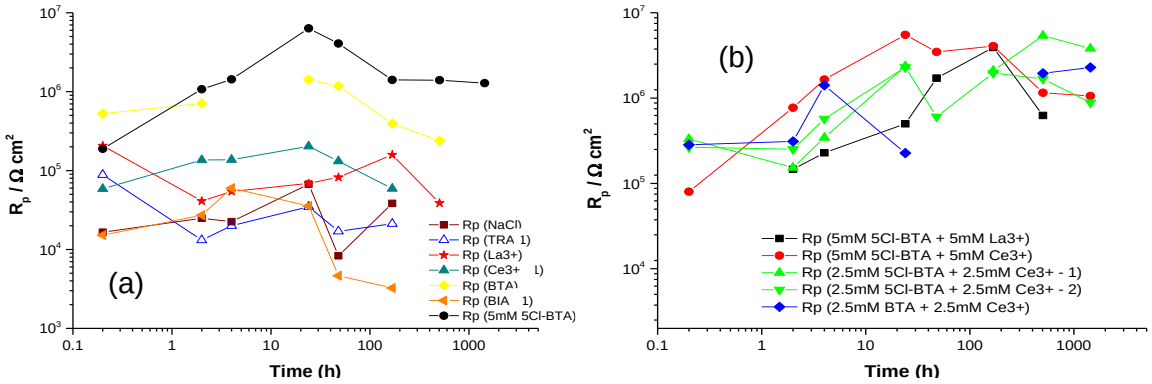

Figure 22 - Evolution of R_p vs. time (h) for **(a)** all inhibitors and **(b)** inhibitor combination systems for AA2024.

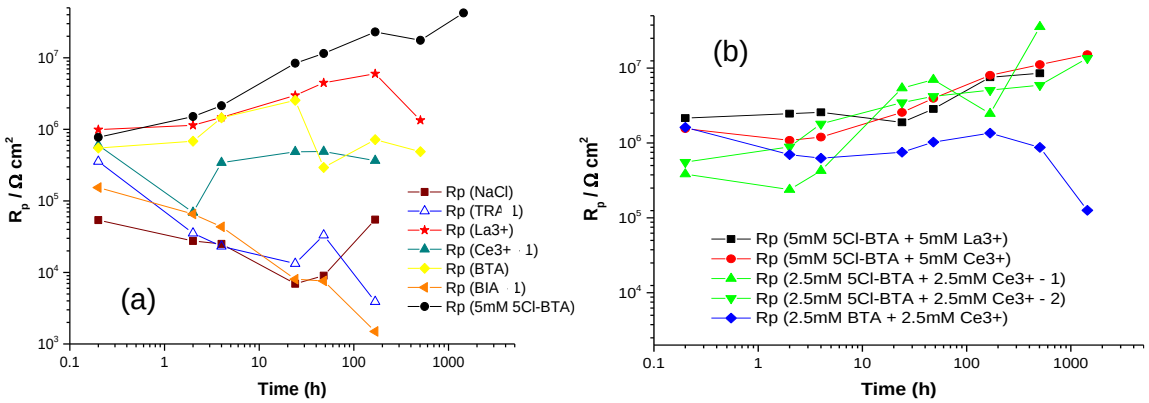

Figure 23 - Evolution of R_p vs. time (h) for **(a)** all inhibitors and **(b)** inhibitor combination systems for AA2198.

It can be concluded that the R_p values tend to behave rather equally (with only few exceptions) to low frequency impedance ($|Z|_{0.1Hz}$) which also points to the sufficient fitting quality

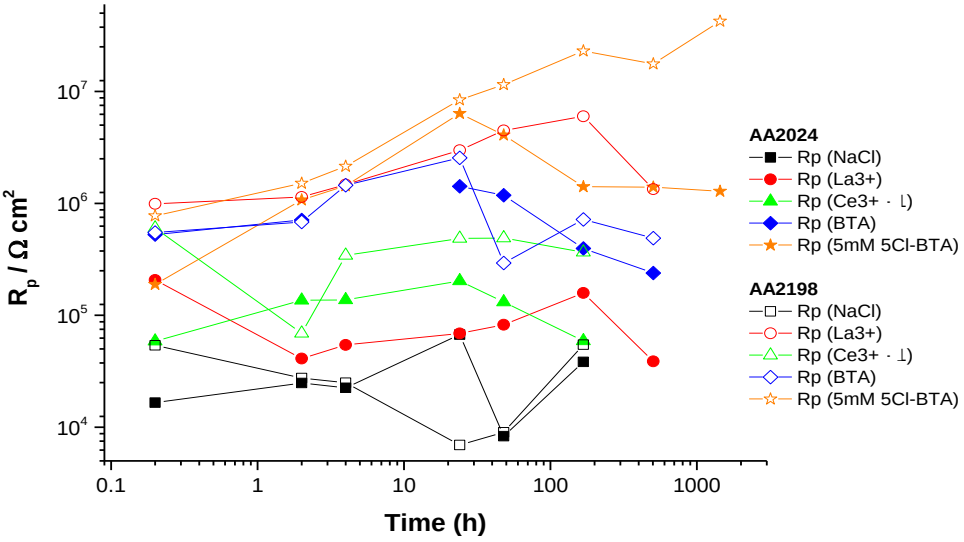

Figure 24 - Evolution of R_p vs. time (h) for both alloys with selected single inhibitors.

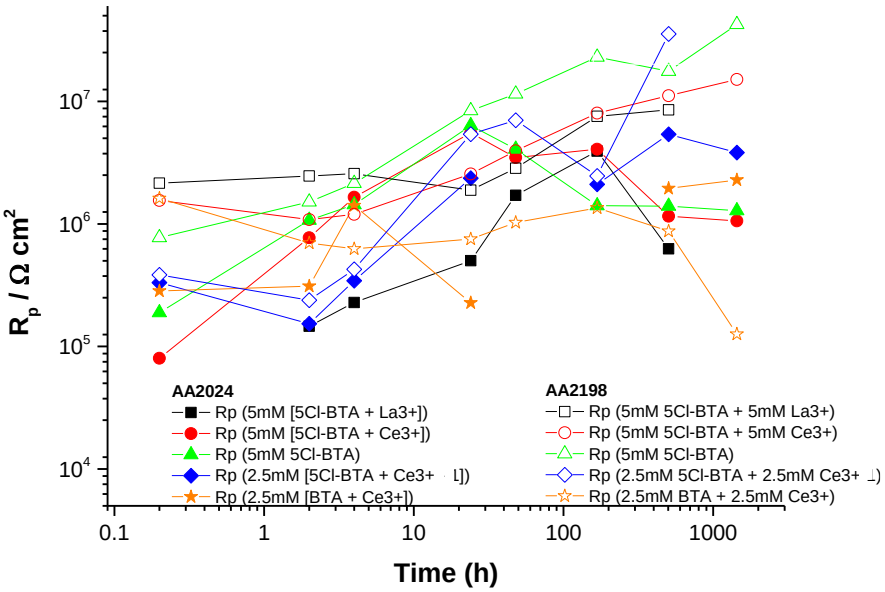

Figure 25 - Evolution of R_p vs.time (h) for both alloys with 5Cl-BTA and 3 selected inhibitor combinations.

In the case of R_p (Figures 24 and 25) the same behaviour of both alloys appears as for the Low Frequency ($|Z|_{0.1Hz}$) pointing to generally lower corrosion activities on AA2198 compared to AA2024.

The overall EIS data analysis permitted to conclude that amongst all tested inhibitor systems the *5mM 5Cl-BTA*, *5mM [5Cl-BTA + Cerium (III) Nitrate]* and *5mM [5Cl-BTA + Lanthanum (III) Nitrate]* are the most suitable systems for corrosion mitigation on AA2024 and AA2198 substrates in chloride containing media.

4.1.2 SVET

In parallel to the study done with EIS (an integral electrochemical technique), SVET was also used with the objective of testing and identifying localised corrosion activities on the metals' surfaces. SVET helps to study more closely the localised corrosion activities and its suppression on these alloys with implementation of corrosion inhibitors (all those used also in EIS study).

The objective was to systematically screen and analyse the different SVET maps and currents given by each sample. For such study different samples from each alloy were prepared and immersed separately in all inhibitor systems prepared. The expectance was to track the differences on the resulting ionic activities of each system and their differences with respect to the reference solution. This approach provides significant help in order to understand if the added inhibitors work to mitigate the localized corrosion processes on the AA substrates immersed in chloride containing media. Table 8 presents few SVET maps of AA2024 and AA2198 electrodes immersed in reference solution and with addition of 3 selected inhibitors. These maps show the values of both anodic and cathodic activities (colours red and blue respectively) close to the sample's surface. It can be seen that when added to reference solution, the presented inhibitor systems tendentiously decrease the activities on the samples surfaces which points to their efficiency in terms of corrosion mitigation.

Also Figures 26 and 27 are presented as a second approach in order to show the evolution of the measured values of maximum anodic currents (where the dissolution of the metal is taking place) through time for both alloys. The plotted values will also help to understand if and for how long the selected inhibitors work on corrosion suppression.

Table 7 – SVET maps and photographs of time evolution for both alloys immersed in different inhibitor mediums + 0.05M NaCl

	AA2024			AA2198		
	4 hours	1 day	2 days	4 hours	1 day	2 days
0.05M NaCl	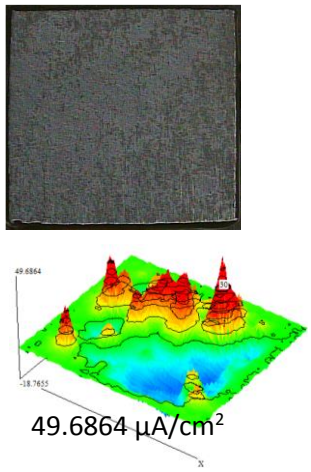 49.6864 µA/cm^2	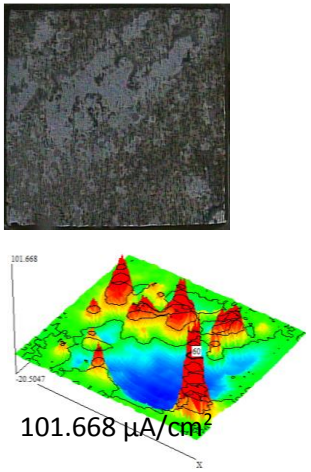 101.668 µA/cm^2	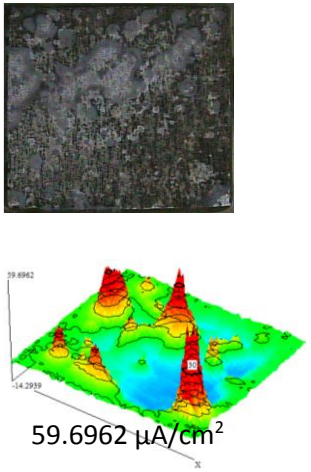 59.6962 µA/cm^2	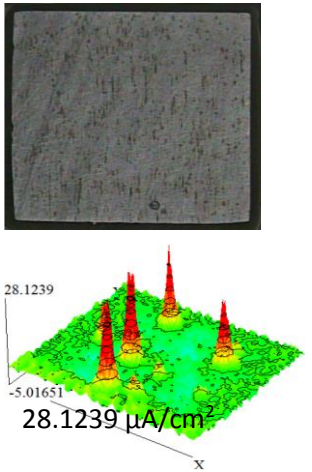 28.1239 µA/cm^2	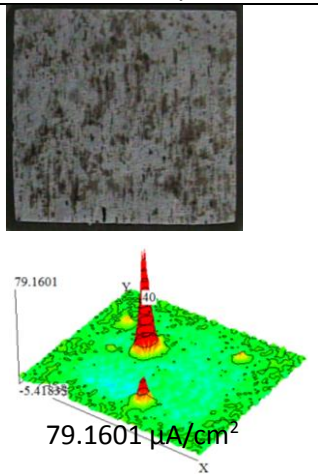 79.1601 µA/cm^2	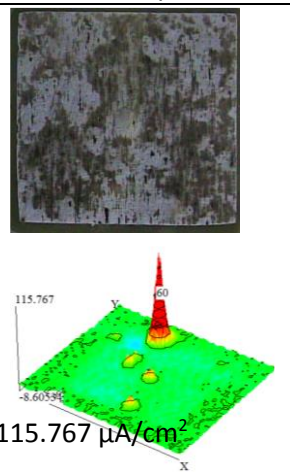 115.767 µA/cm^2
5mM 5Cl-BTA	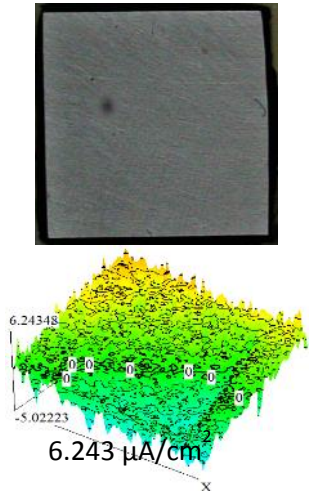 6.243 µA/cm^2	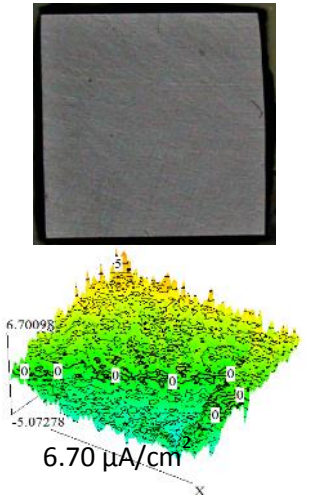 6.70 µA/cm^2	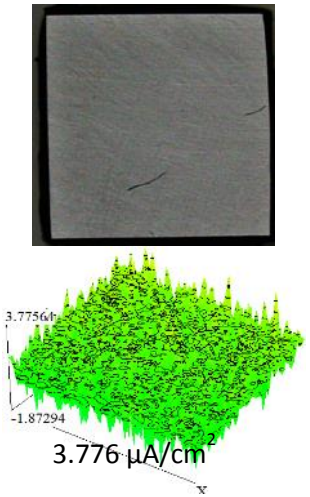 3.776 µA/cm^2	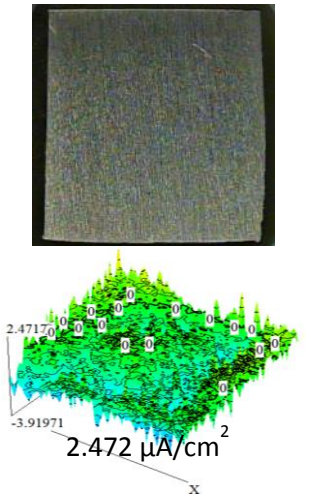 2.472 µA/cm^2	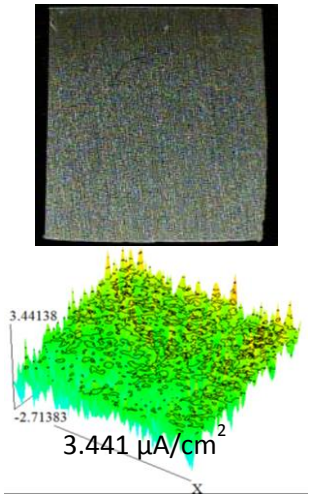 3.441 µA/cm^2	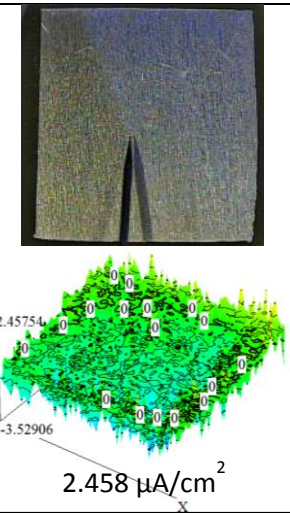 2.458 µA/cm^2

5mM Lanthanum (II) Nitrate	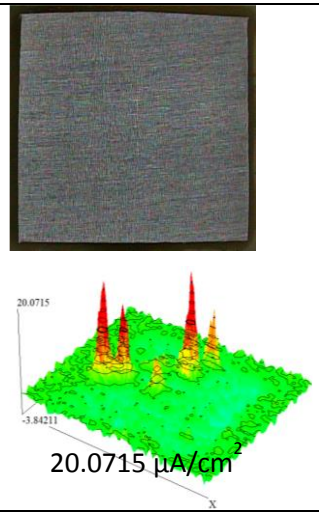 20.0715 µA/cm^2	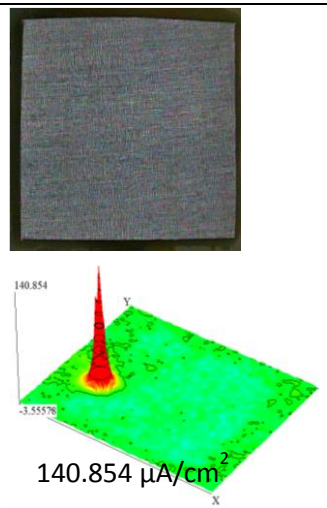 140.854 µA/cm^2		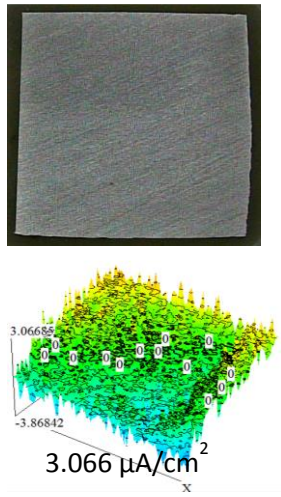 3.066 µA/cm^2	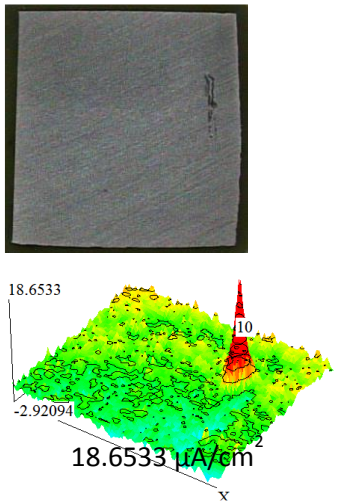 18.6533 µA/cm^2	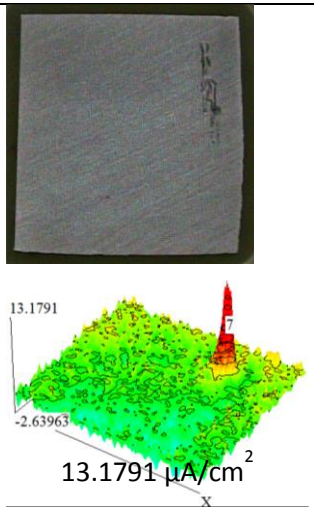 13.1791 µA/cm^2
2.5mM [5Cl-BTA + Cerium Nitrate	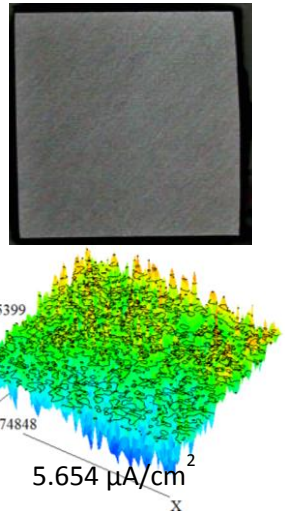 5.654 µA/cm^2	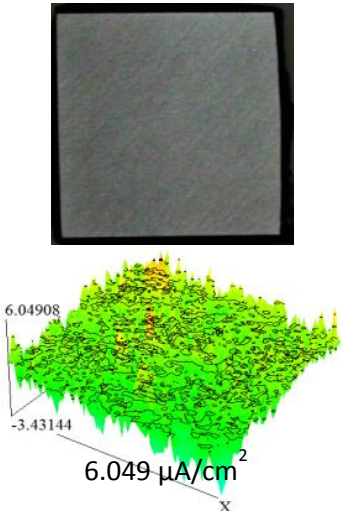 6.049 µA/cm^2	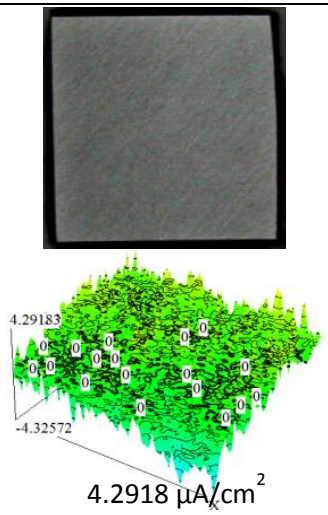 4.2918 µA/cm^2	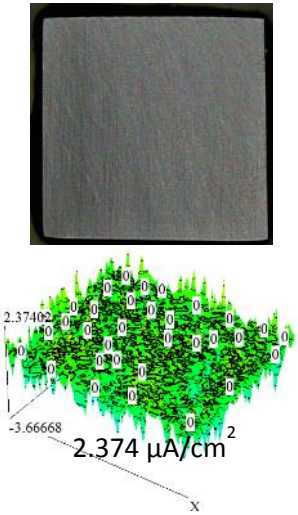 2.374 µA/cm^2	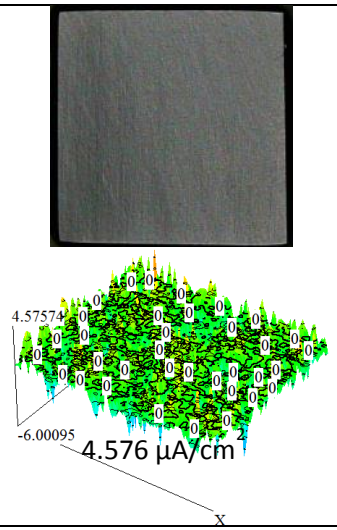 4.576 µA/cm^2	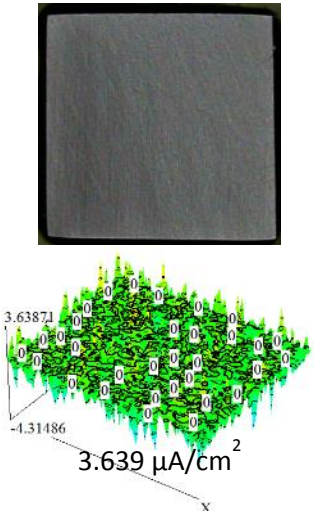 3.639 µA/cm^2

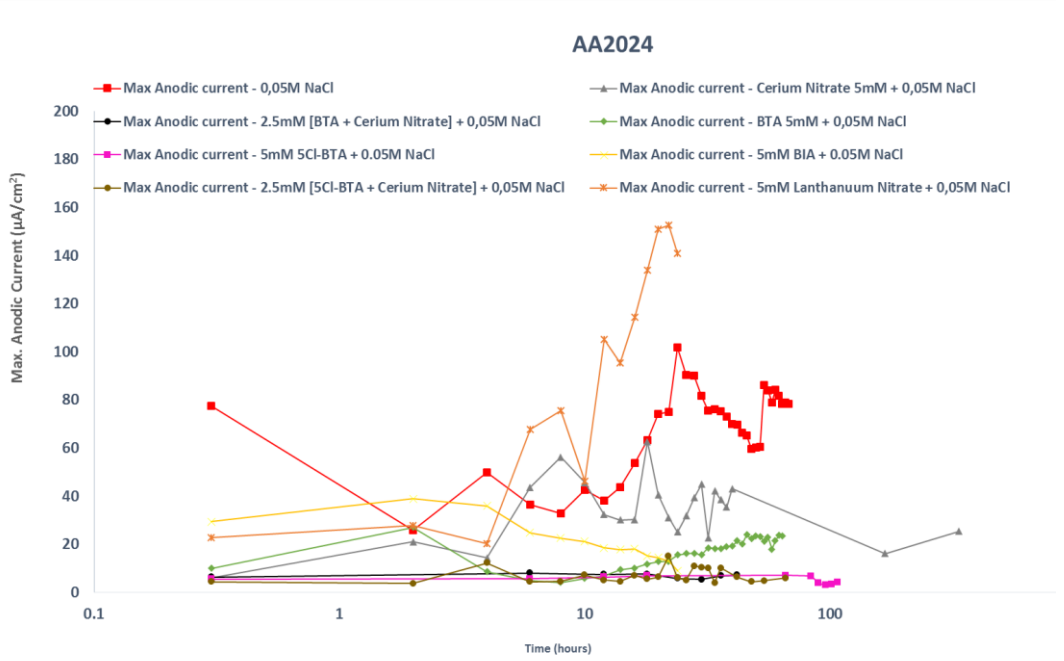

Figure 26 Evolution of Maximal Anodic activities on AA2024 immersed in different mediums (Reference + Inhibitors)

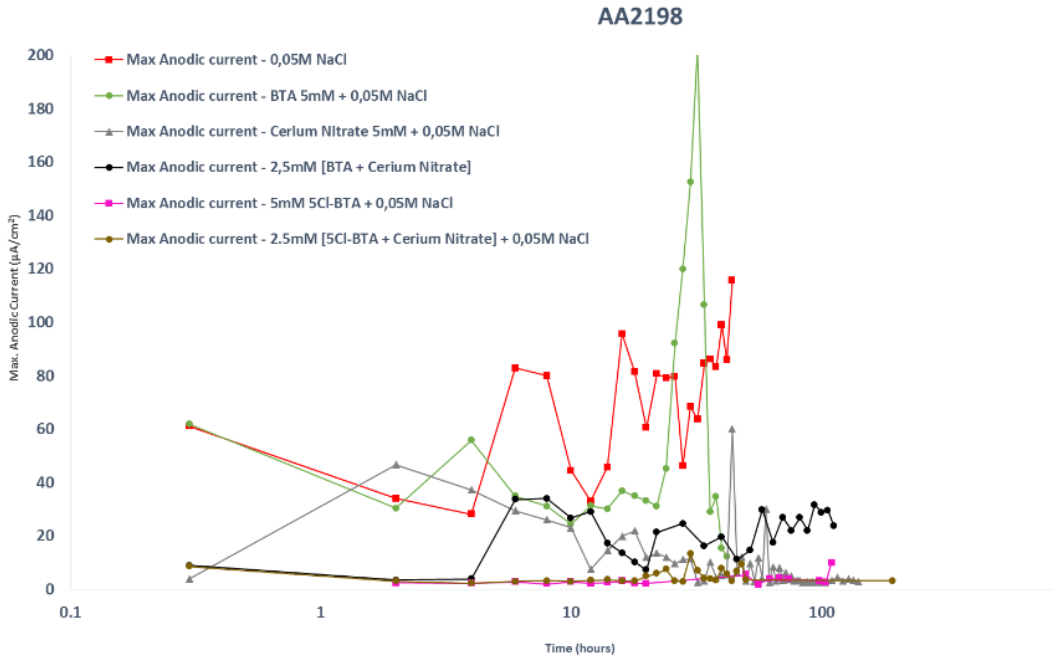

Figure 27 - Evolution of Maximal Anodic activities on AA2198 immersed in different mediums (Reference + Inhibitors)

Based on the results given above in Figures 26 and 27 it is possible to visualize that from the tested inhibitors: BIA, Lanthanum (III) Nitrate and Cerium (III) Nitrate showed high maximal anodic activities in the case of both alloys. The currents are comparable with their

behaviour in 0.05M NaCl reference solution, which points to their poor efficiencies in terms of corrosion suppression for both alloys. On the other hand 5Cl-BTA and 2.5mM [5Cl-BTA + Cerium (III) Nitrate] show better efficiency as the registered ionic currents are rather lower.

An important aspect to underline are the cases of BTA and 2.5mM [BTA + Cerium (III) Nitrate], where results show that both these systems tend to behave fairly better for AA2024. This can be explained by the greater amount of copper in the chemical composition of this alloy, when compared to AA2198 and also to the tendency that BTA has to adsorb specifically to copper surfaces. This behaviour is more visible in Figure 28, where the comparison between the maximum anodic activities of the selected better working systems for each alloy is presented.

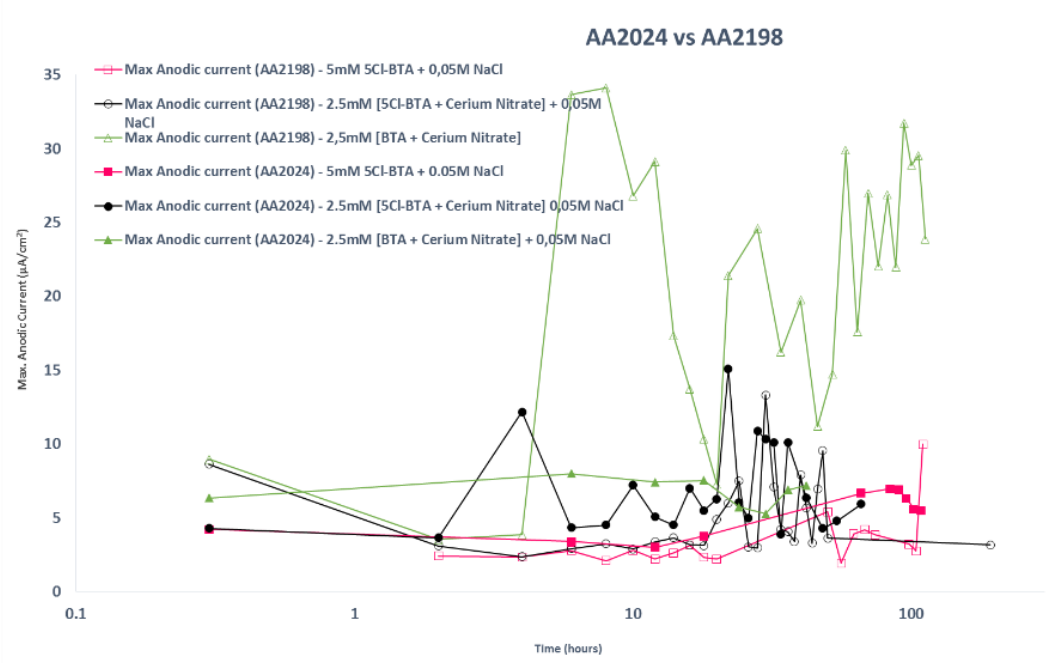

Figure 28 – Comparison of the Evolution of Maximal Anodic activities on both alloys for the selected mediums

Regarding 5Cl-BTA and 2.5mM [5Cl-BTA + Cerium (III) Nitrate] the values of the maximal anodic activities are low (practically very close to the general noise level in SVET-map) and somewhat close to each other, pointing to the good inhibitive properties of these systems when compared to the others.

These results are supported by the data presented in Table 9, where the photos and maps of the 2 alloys immersed in 3 different systems (in comparison with the reference system) are shown for selected immersion times.

4.2 INFLUENCE OF INHIBITOR CONCENTRATION

4.2.1 EIS

The most efficient inhibitor systems based on above EIS and SVET analysis were selected for more specific investigations of inhibitor concentration effect to the protection properties. These were 5Cl-BTA, [5Cl-BTA + Cerium (III) Nitrate] and [5Cl-BTA + Lanthanum (III) Nitrate]. From each of these 5mM initial solutions three dilutions were prepared (10, 100 and 1000 times) with concentrations of 0.5mM, 0.05mM and 0.005mM in 0.05M NaCl media. The results for these concentrations (Low Frequency $|Z|_{0.1Hz}$ and R_p) are presented in Figure 29 and are related to AA2024 and AA2198 respectively.

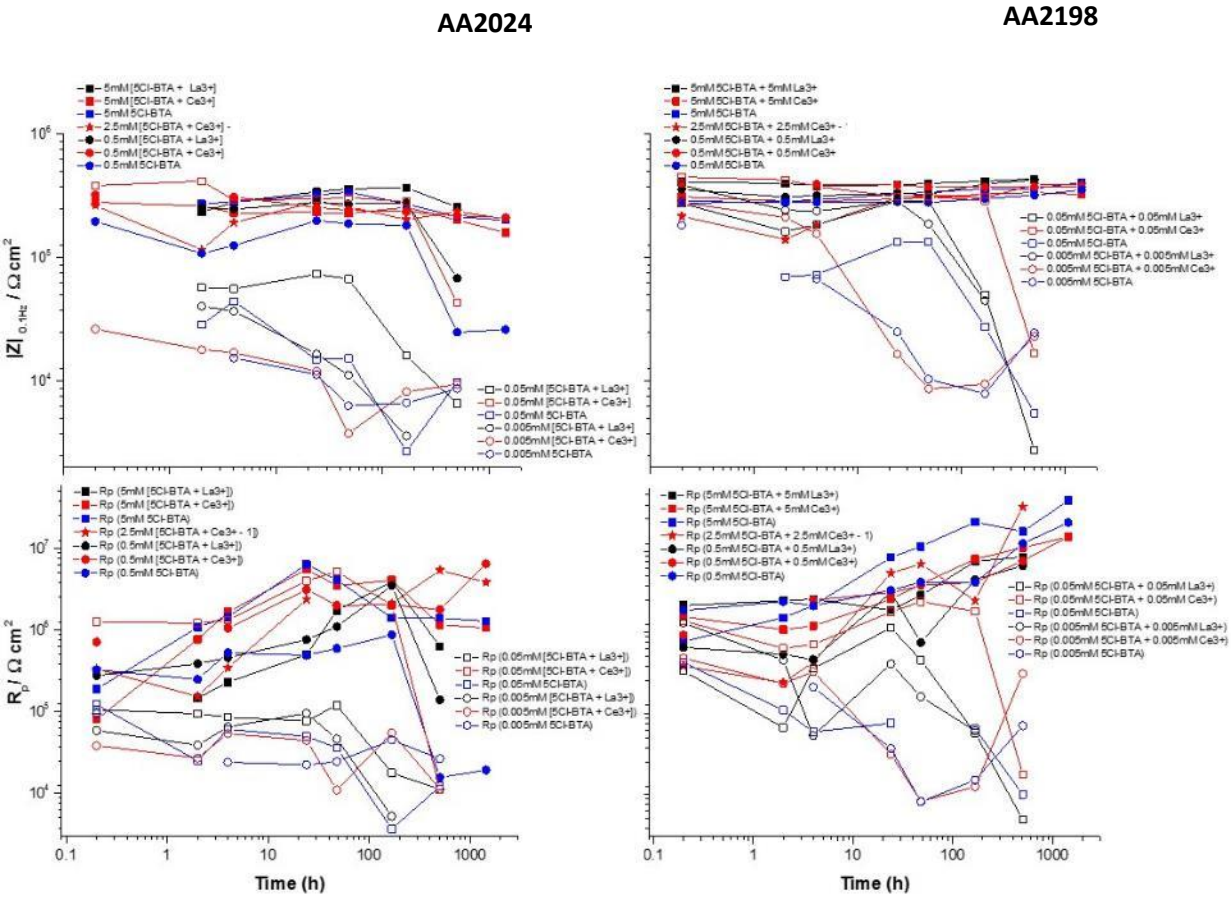

Figure 29 – Low Frequency impedance ($|Z|_{0.1Hz}$) and R_p values vs. time for AA2024 (**left**) and AA2198 (**right**)

The obtained values of $|Z|_{0.1Hz}$ and R_p show that for lower concentrations (0.05 and 0.005mM) none of the selected systems works as efficient corrosion inhibitor when added to the reference solution of 0.05M NaCl. Due to this fact, Figures 30 and 31 are presented

in order to show the differences of these behaviours ($|Z|_{0.1Hz}$ and R_p vs Time) between the used alloys but without data related to those lower concentrations.

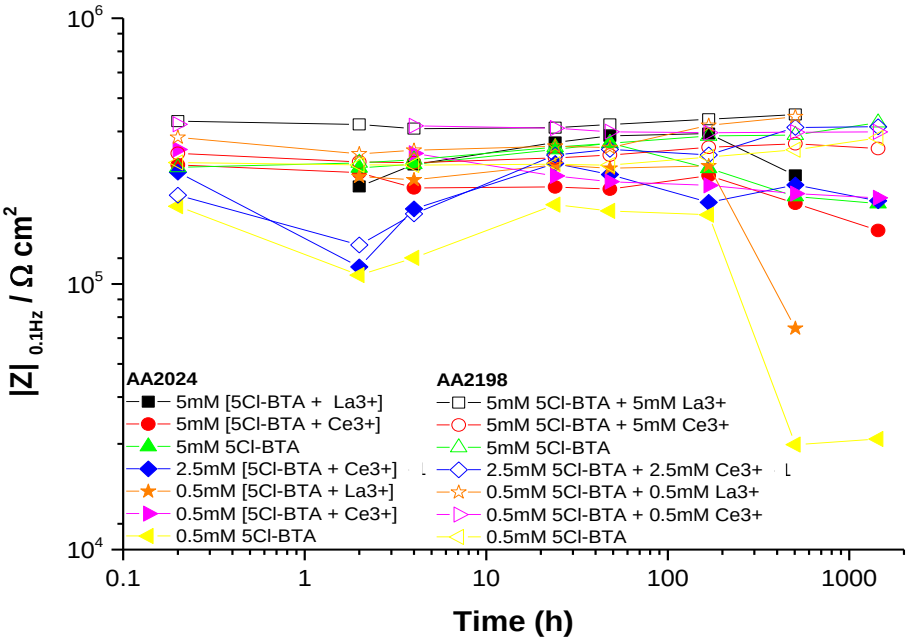

Figure 30 - Evolution of low frequency impedance ($|Z|_{0.1Hz}$) vs. time (h) for both alloys with selected concentrations of inhibitor/inhibitor combinations + 0.05M NaCl.

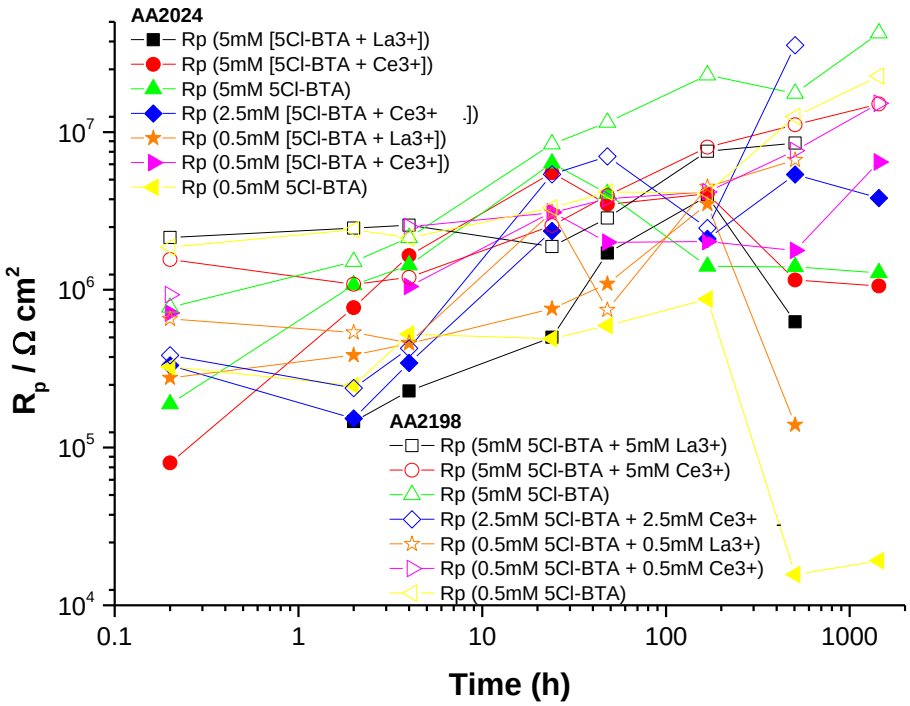

Figure 31 - Evolution of R_p vs. time (h) for both alloys with selected concentrations of inhibitor/inhibitor combinations + 0.05M NaCl.

As well as for primary inhibition study, the results here also point to somewhat lower corrosion activities on AA2198 compared with AA2024.

In order to understand how the inhibitors concentrations influence in the corrosion inhibition of these alloys (and compare the behaviours for each of them), four selected times of immersion (4 hours, 2 days, 1 week and 3 weeks) were chosen and the evolution of both $Z|_{0.1Hz}$ and R_p vs Concentration (mM) were presented in Figures 32 and 33 respectively.

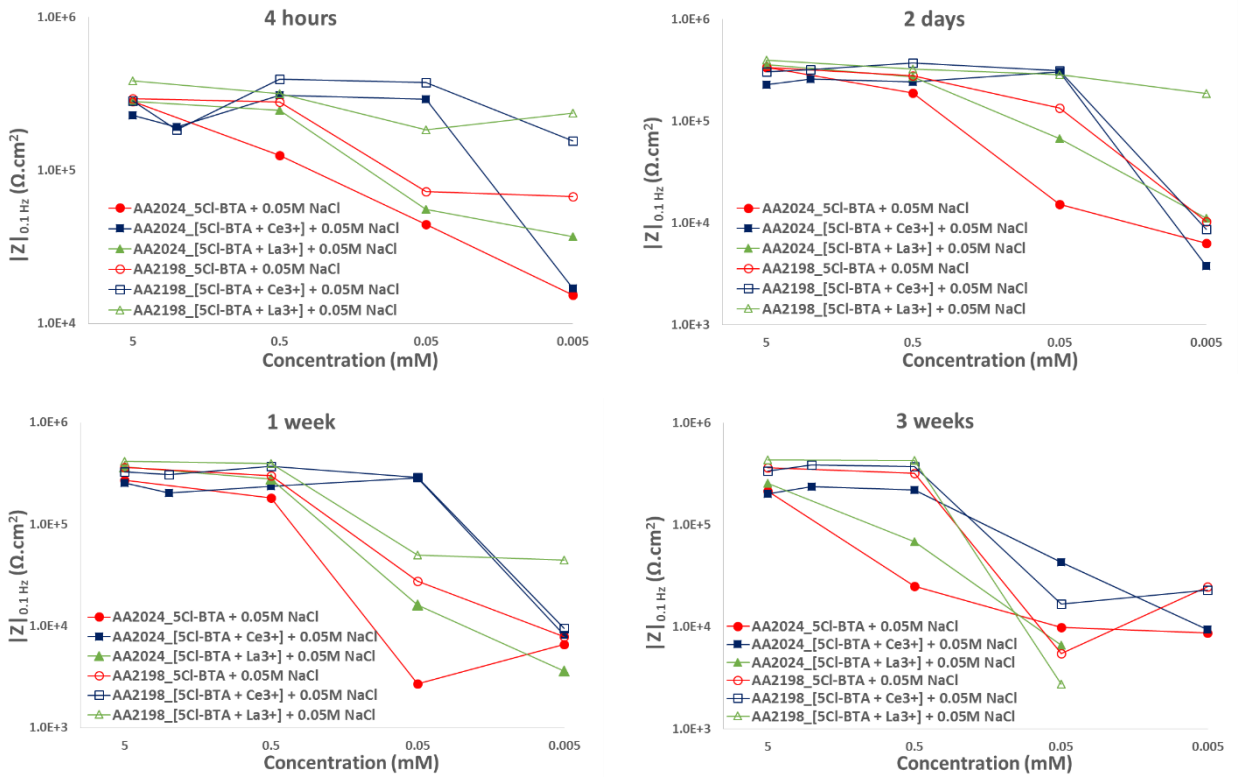

Figure 32 - Evolution of low frequency impedance ($|Z|_{0.1Hz}$) vs. concentration (mM) for both alloys for the selected immersion times (4 hours, 2 days, 1 and 3 weeks).

From the plots given above it is possible to see that the values of |Z| for both alloys are higher (in the selected time range) for concentrations over 0.5mM (in the case of inhibitors combination solutions). While, the 0.05mM solutions demonstrate good inhibitive behaviour for a significant period, then on 1 week point the efficiency is no longer visible. However, both alloys immersed in 0.05mM 5Cl-BTA + Ce3+ are the exceptions in this case. Such situation may be related with the lower thickness of the inhibitive adlayer (less amount of inhibitors in solution capable to adsorb on the metal surfaces) formed with lower concentrations. Another point to underline is the fact that at 2 days, the majority of the lower concentration solutions (0.005mM) stop working at all with the exception of AA2198

immersed in 0.005mM 5Cl-BTA + Lanthanum (III) Nitrate, which still continues to perform efficiently at this period of immersion..

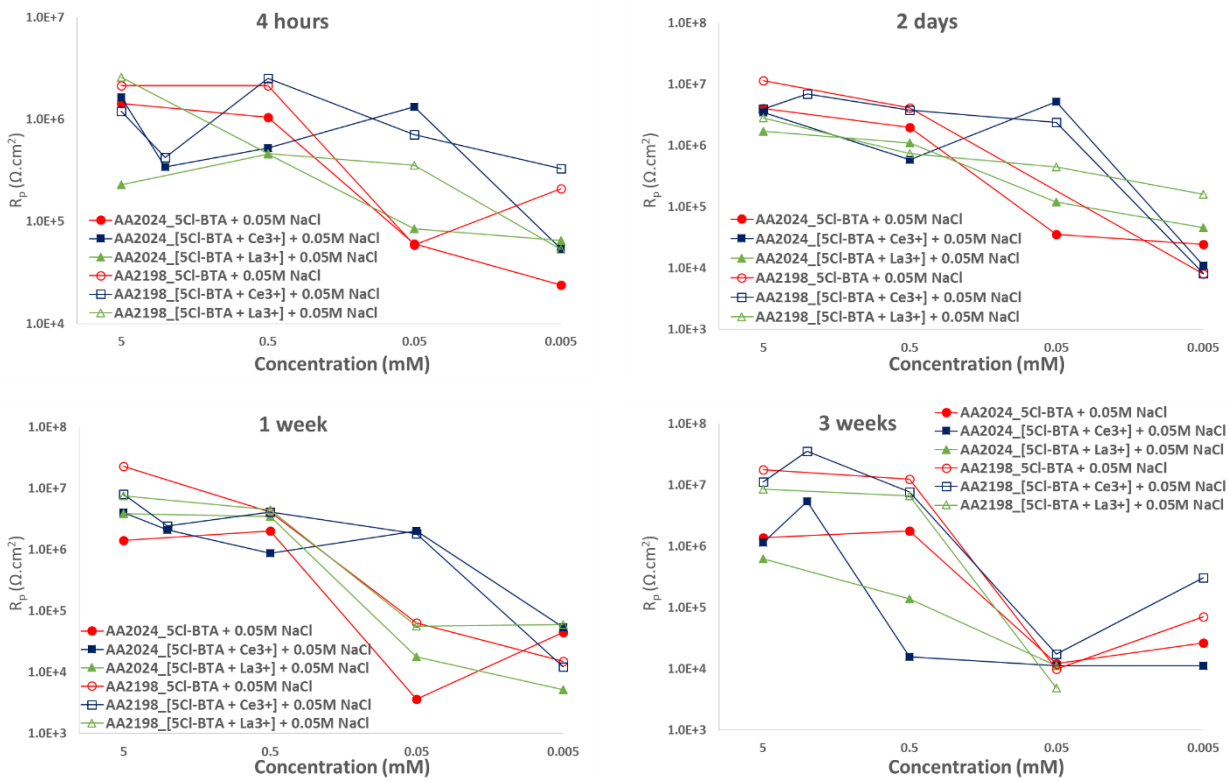

Figure 33 - Evolution of R_p vs. concentration (mM) for both alloys for the selected immersion times (4 hours, 2 days, 1 and 3 weeks).

The analysis of the evolution of the R_p values is somewhat analogue to that done regarding the evolution of $|Z|_{0.1Hz}$ vs. concentration (mM). The best inhibitive performances are observed in the case of the solutions with inhibitor concentrations above 0.5mM. As well as above, the case of inhibitors combinations seem to work better than single inhibitors.

An overall consideration is the observation that all these systems seem to work slightly better for AA2198 when compared with AA2024.-

4.2.2 SVET

As it was done for the inhibitor systems study, SVET was also used to investigate the effect of concentration the corrosion inhibition performance on both alloys immersed in 0.05M NaCl. The same approach has been applied regarding the map and graphic presentations. In Table 9, the SVET maps for selected immersion times of both alloys in different mediums are presented. Just a couple of the tested solutions are listed in this table. As for the graphic presentation, all concentrations of the three different inhibitor systems

are shown first separately regarding the immersed alloys (Figures 34 and 35) and the comparison between alloys (Figure 36) for the best performing systems.

Table 8 - SVET maps and photographs related to the given immersion times for both alloys in different inhibitor mediums + 0.05M NaCl

	AA2024		AA2198	
	4 hours	1 day	4 hours	1 day
0.5mM 5Cl-BTA	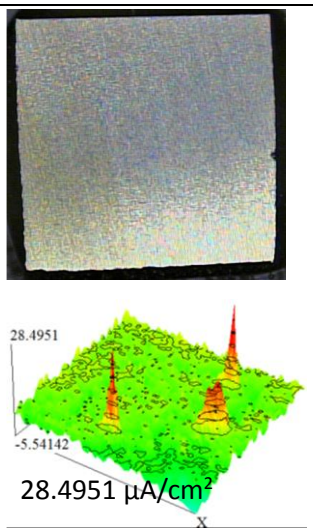	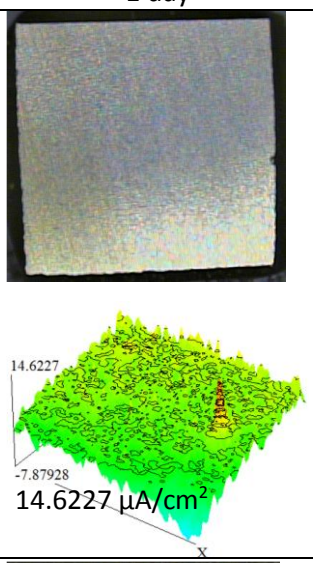		
0.5mM [5Cl-BTA Lanthanum (III) Nitrate]	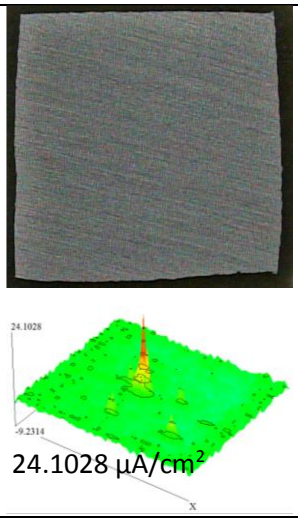	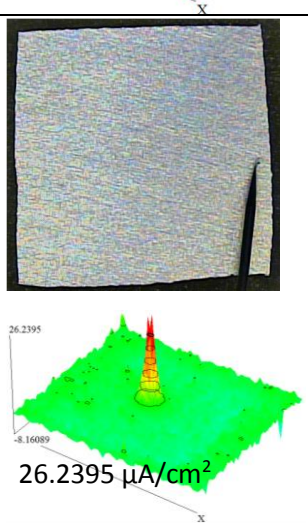	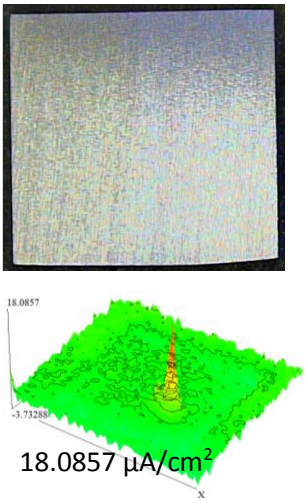	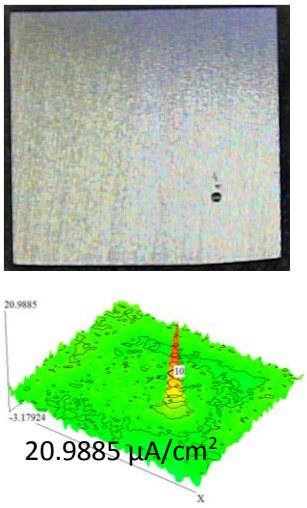
0.5mM [5Cl-BTA Cerium (III) Nitrate]	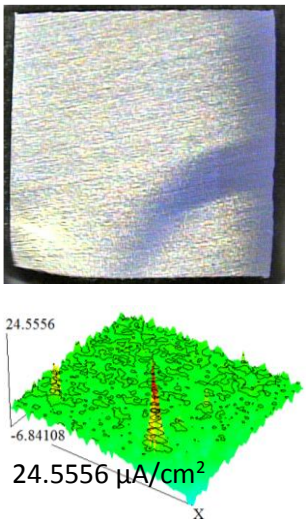	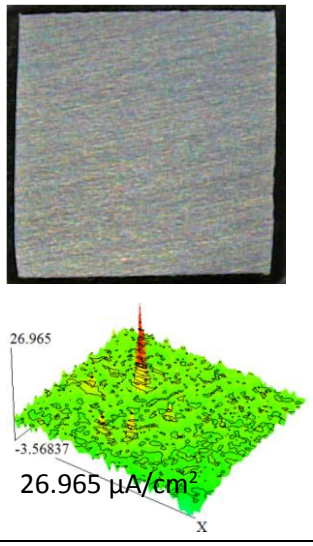	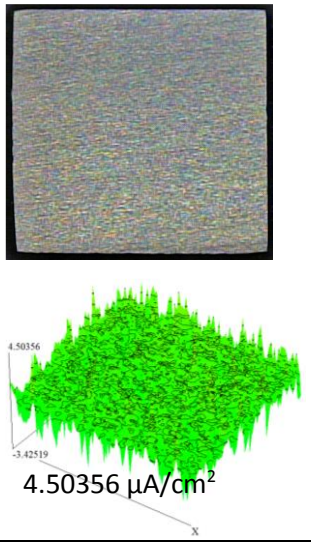	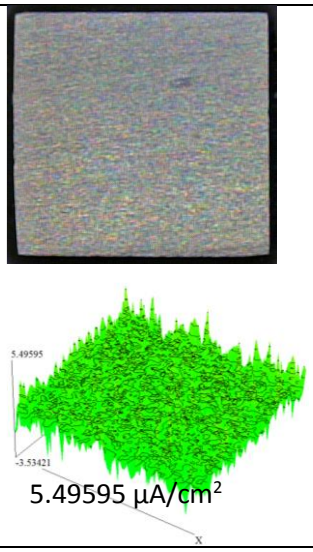

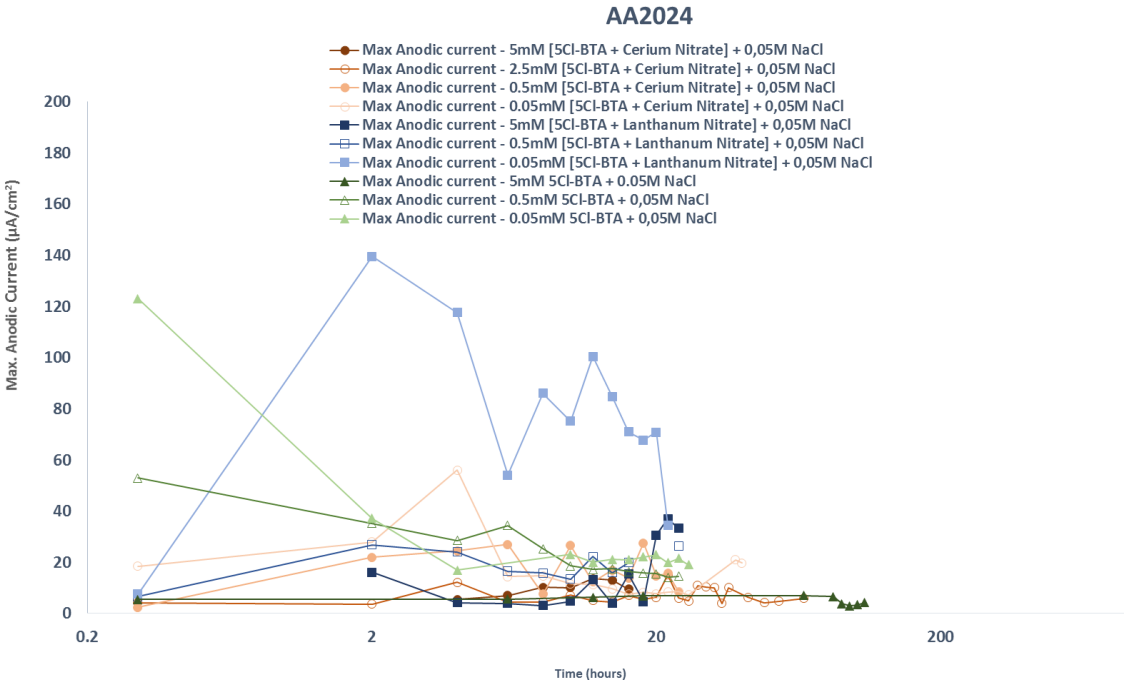

Figure 34 – Evolution of Maximal Anodic activities on AA2024 immersed in different inhibitors concentrations (selected systems)

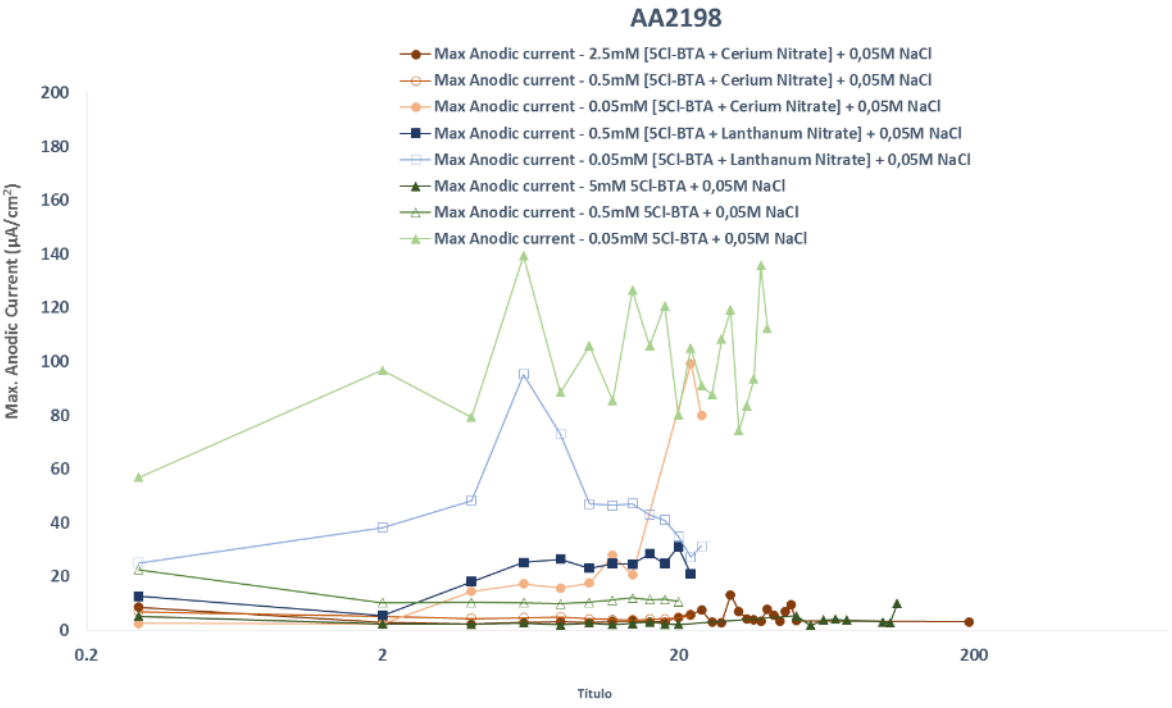

Figure 35 - Evolution of Maximal Anodic activities on AA2198 immersed in different inhibitors concentrations (selected systems)

Analysing Figures 34 and 35 it can be seen that for lower inhibitor concentrations (0.05mM) the maximal anodic activities are relatively higher when compared to more concentrated systems, which shows the non-effectiveness of this concentration for the selected inhibitors for both alloys. For technical reasons (maps with high associated noise values) data related with the inhibitor solutions of 2.5 and 5mM [5Cl-BTA + Lanthanum (III) Nitrate] were not successfully achieved for AA2198 and therefore are not plotted in Figure 35.

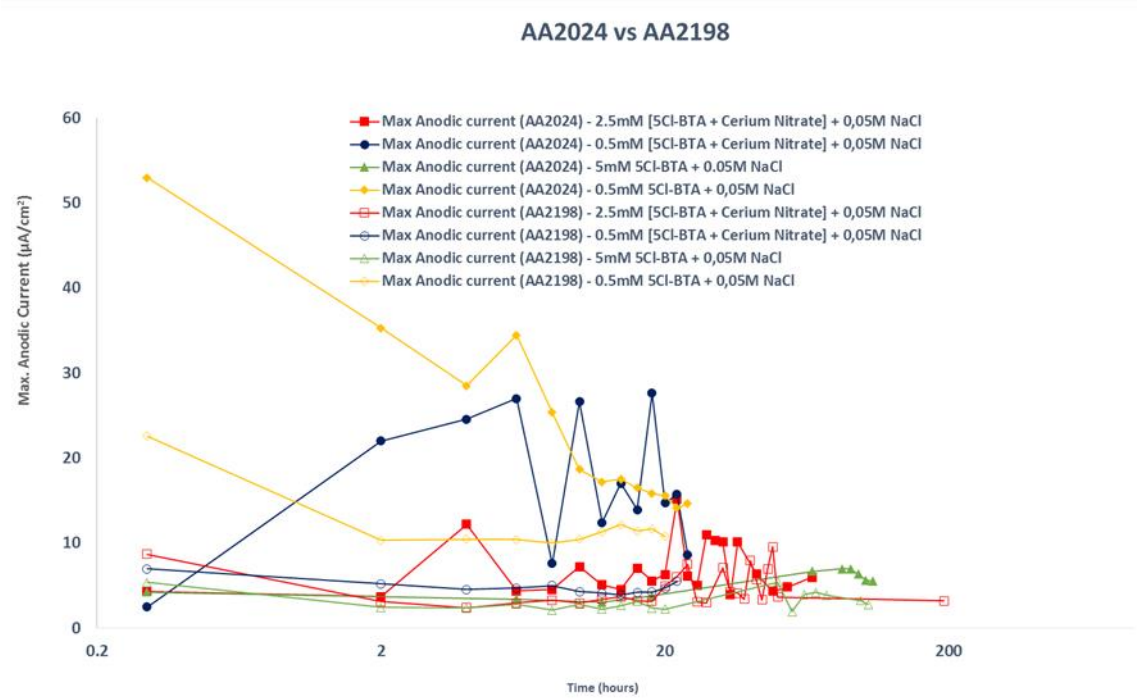

Figure 36 - Evolution of Maximal Anodic activities for both alloys in selected mediums and concentrations

In Figure 36 the comparison between the maximal anodic activities is given for each alloy related with the selected inhibitor concentrations. It is clearly visible that for the lower concentrations (0.5mM) the values of the maximal anodic activities for both 5Cl-BTA and 5Cl-BTA + Cerium (III) Nitrate are slightly lower in the case AA2198. Although less significantly this behaviour is also seen for higher concentrations which is again related with the differences in the chemical composition of these alloys. When immersed in a corrosive medium AA2198 shows less activity than AA2024 which implies that the inhibitors will form a more efficient barrier. It can also be concluded that only for higher concentrations (5 and 2.5mM) this barrier is sufficient to work rather equally for both alloys.

5. CALCULATIONS

5.1 ESTIMATION OF CORROSION LOCALIZATION PARAMETER

In order to understand how dangerous the localized corrosion can be for these substrates, the trial for definition of an empirical parameter based on the results from SVET maps (different spikes with different values of activities, shapes, etc.) with the localized attack has been implemented. The objective was to establish a relationship between all aspects that can influence the value/character of that attack. This led to the following equation:

$$L = N_t * I_{an\,(Max)} / N_{rms} * 1000 \qquad (12)$$

Table 9 – SVET maps and related values of the Localization Parameter (L), the maximum anodic current (I_{max} An.) and the sum of absolute integrated values of current ($I_{sum\ dif}$ ABS)

	AA2024			AA2198		
	SVET map			SVET map		
NaCl (24 hours)	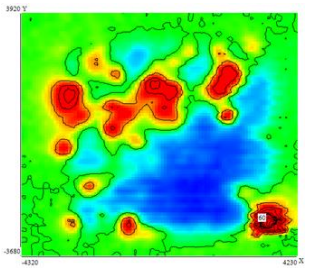	**L**	7.943	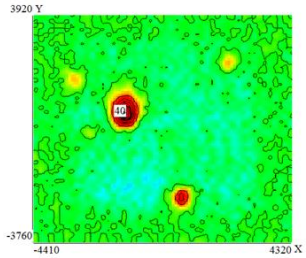	**L**	8.995
		I_{max} An.	101.7		**I_{max} An.**	79.16
		$I_{sum\ dif}$ ABS	4.191		**$I_{sum\ dif}$ ABS**	0.583
BIA (24 hours)	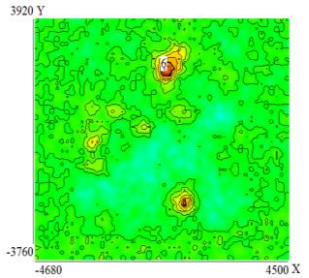	**L**	0.746	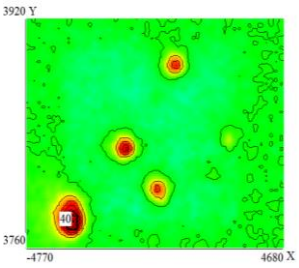	**L**	6.050
		I_{max} An.	8.947		**I_{max} An.**	87.12
		$I_{sum\ dif}$ ABS	0.138		**$I_{sum\ dif}$ ABS**	1.062
$La(NO_3)_3$ (24 hours)	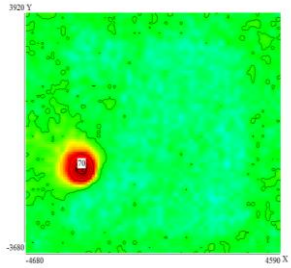	**L**	20.71	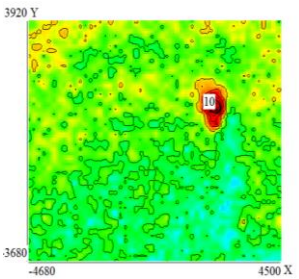	**L**	1.943
		I_{max} An.	140.9		**I_{max} An.**	18.65
		$I_{sum\ dif}$ ABS	0.530		**$I_{sum\ dif}$ ABS**	0.149

, where *L* is the Localized Activity Index, N_t is the total number of data points, $I_{an\ (Max)}$ is the maximum anodic current, and N_{rms} is the number of data points where the anodic currents exceed 3 times the general RMS noise value.

Table 10 shows the results given by this parameter for some of the resulting maps of the tested solutions for a specific immersion time and the comparison between the used alloys.

It can be seen in Table 10 that in the cases where clear differences are visible regarding the amount of corrosion activities in each map these differences also appear in the value of the localized activity index **L**. Another aspect is that high values of $\mathbf{I_{max}}$ **An.** lead to high values of **L** as well as the sum of the absolute integrated values of current ($\mathbf{I_{sum\ dif}}$ **ABS**) plays its role. This value can tell something about the Localization parameter in the way that it is higher in the cases with more activities. With AA2024 the anodic activities are more homogeneously spread in the surface area which is not the case here (0.05M NaCl reference solution) for AA2198, where only 2 prevailing peaks dominate. This also explains the higher value of **L**, thus indicating a more dangerousness situation due to the higher tendency for the occurrence of the localized attack.

The same can be said in the case of immersed alloys in BIA containing solution where the presence of more localized and significant peaks for AA2198 are visible and also the value of the peaks themselves are rather higher, which explains its higher value of the **L** parameter.

For the case of both aluminium alloys immersed in Lanthanum (III) Nitrate the sum of the absolute integrated values of current ($\mathbf{I_{sum\ dif}}$ **ABS**) indicate few activities at their surfaces and the value of $\mathbf{I_{max}}$ **An.** is higher in the case of AA2024 when compared with AA2198 thus resulting in higher value of **L** for AA2024 than for AA2198

This is a very interesting approach and requires more systematic testing and parameter development in the future

5.2 CALCULATION OF INHIBITOR EFFICIENCIES

The objective of this part of the work was the numerical assessment of Inhibitor Efficiencies for all tested systems. The equation 13 [13] has been applied.

$$IE = CR_0 - CR_{Inh} / CR_0 \qquad (13)$$

, where *IE* is the Inhibitor Efficiency, CR_0 is the corrosion rate of the non-inhibited system and CR_{Inh} is the corrosion rate of the inhibited system.

In order to calculate the *IE*, there is the need to define the various corrosion rates for all tested systems. To do so, different approaches can be considered based on the results of systematic electrochemical analysis (Table 11).

Table 10 – Parameters used to calculate the Corrosion Rates of the tested systems

	EIS
CR	$1 / \lvert Z \rvert_{0.1\ Hz}$
	$1 / R_p$

All calculations were done for the cases of inhibitor systems variation and for the study of the concentration effect (Figures 37 and 38).

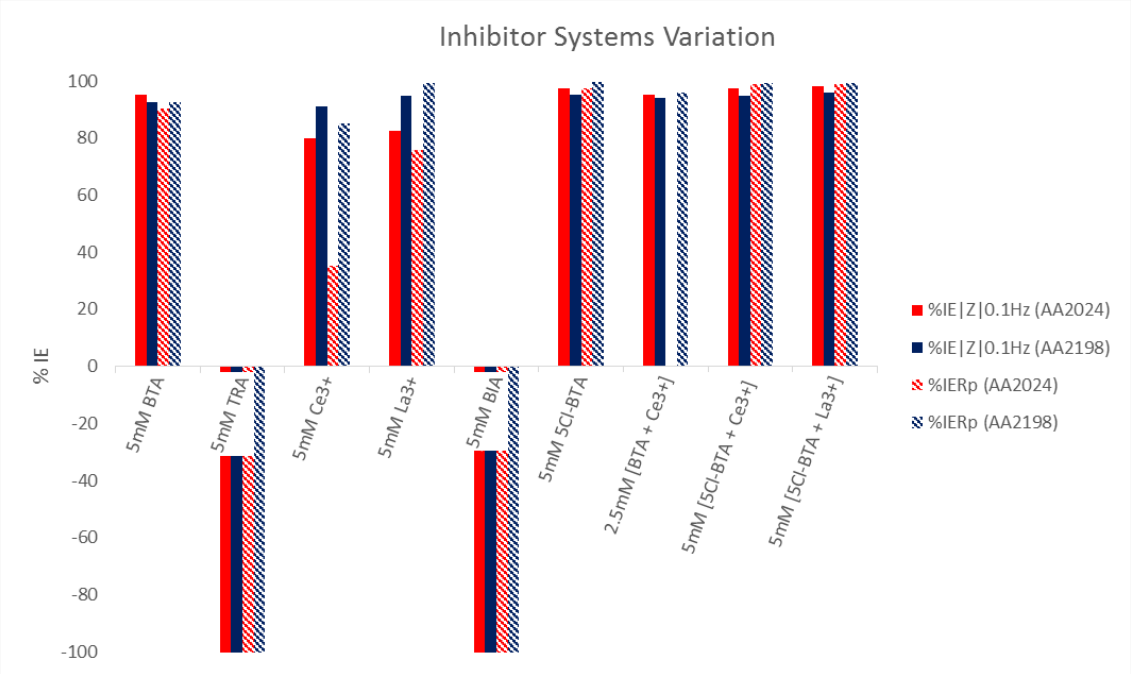

Figure 37 - Inhibition efficiencies for both alloys obtained from $\lvert Z \rvert_{0.1Hz}$ and R_p in various environments

Regarding the study of the inhibitor systems variation (Figure 37) it is clear that neither TRA nor BIA work as corrosion inhibitors for these alloys in 0.05M NaCl. Another important aspect is that for systems containing BTA or 5Cl-BTA the Inhibitor Efficiencies are higher for the case of AA2024. This higher effect for AA2024 comes from the more active reference system (0.05M NaCl) when compared to AA2198 which is already less active in the reference solution. The resulting inhibitor efficiencies (for $\lvert Z \rvert_{0.1Hz}$ and R_p)

values are rather similar which points to a mathematically higher value of *IE* for AA2024. The extracted values from the plot (%IE) can be seen in Table 12.

Table 11 - % IE for AA2024 and AA2198 calculated from $|Z|_{0.1Hz}$ and R_p (Inhibitor systems variation)

Inhibitors	$\%IE_{\|Z\|0.1Hz}$ (AA2024)	$\%IE_{\|Z\|0.1Hz}$ (AA2198)	$\%IE_{Rp}$ (AA2024)	$\%IE_{Rp}$ (AA2198)
5mM BTA	95.30	92.49	90.29	92.38
5mM TRA	-320.84	-300.08	-1903.50	-1301.37
5mM Ce3+	79.73	90.87	35.08	85.07
5mM La3+	82.65	94.81	75.78	99.09
5mM BIA	-308.87	-1635.11	-1081.79	-3558.08
5mM 5Cl-BTA	97.43	95.19	97.28	99.76
2.5mM [BTA + Ce3+]	95.16	94.11	0.00	95.96
5mM [5Cl-BTA + Ce3+]	97.27	94.69	99.06	99.32
5mM [5Cl-BTA + La3+]	98.10	95.83	99.02	99.28

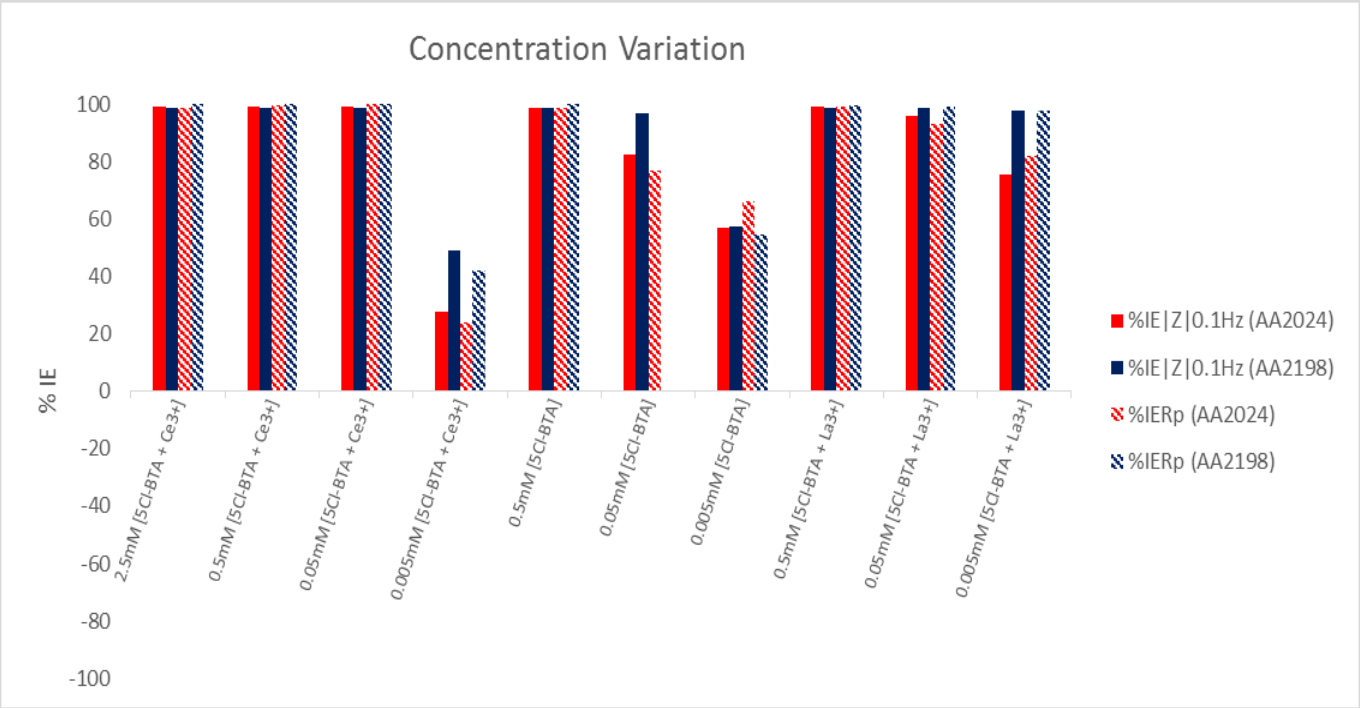

Figure 38 – Effect of the inhibitors concentrations on the % of the Inhibitors Systems Efficiencies for both alloys obtained for $|Z|_{0.1Hz}$ and R_p

The study of the effect of inhibitors concentration (Figure 38) led to the conclusion that generally the systems under 0.05mM concentration do not show good performance except 5Cl-BTA + Lanthanum (III) Nitrate on AA2198 which also works sufficiently in the

0.005mM inhibitors concentration. This happens because Lanthanum (III) Nitrate has more tendency to complex and form hydroxides in more lithium containing alloys with is the case of AA2198. Regarding the other systems and systems concentrations all seem to work as corrosion inhibitors, for which maybe longer immersion times in further experiments should be considered in order to track possible differences and have more conclusive understanding of their inhibition performances. As it was done in the case of the inhibitor systems variation, Table 13 shows the values which are related to the plot presented in Figure 38.

Table 12 - % IE for AA2024 and AA2198 calculated from $|Z|_{0.1Hz}$ and $R_{p.}$ (Concentration Variation)

Inhibitors	$\%IE_{\|Z\|0.1Hz}$ (AA2024)	$\%IE_{\|Z\|0.1Hz}$ (AA2198)	$\%IE_{Rp}$ (AA2024)	$\%IE_{Rp}$ (AA2198)
2.5mM [5Cl-BTA + Ce3+]	98.95	98.63	98.63	99.95
0.5mM [5Cl-BTA + Ce3+]	98.88	98.82	99.58	99.90
0.05mM [5Cl-BTA + Ce3+]	99.12	98.59	99.84	99.84
0.005mM [5Cl-BTA + Ce3+]	27.78	49.02	24.16	42.02
0.5mM [5Cl-BTA]	98.56	98.43	98.60	99.91
0.05mM [5Cl-BTA]	82.27	96.71	76.86	0.00
0.005mM [5Cl-BTA]	56.99	57.38	65.92	54.66
0.5mM [5Cl-BTA + La3+]	99.00	98.65	99.24	99.49
0.05mM [5Cl-BTA + La3+]	95.96	98.46	93.05	99.16
0.005mM [5Cl-BTA + La3+]	75.63	97.65	82.02	97.61

6. CONCLUSIONS

- The corrosion protection of two different aluminium alloys (AA2024 and AA2198) in chloride containing environment was systematically investigated by combining EIS and SVET techniques in order to obtain quantitative and localized information of the occurring corrosion processes. The development and screening of suitable corrosion inhibition strategies was the main goal of the work.

- The addition of different inhibitors and inhibitor combinations was tested and systematically analysed.

- The comparison of data gathered with EIS (low frequency impedance $|Z|_{0.1Hz}$ and R_p) and SVET (maximum anodic ionic currents) allowed to conclude that amongst all inhibitor systems studied, 5Cl-BTA, 5Cl-BTA + Cerium (III) Nitrate and 5Cl-BTA + Lanthanum (III) Nitrate were those that presented higher corrosion inhibiting performance.

- As a single inhibitor 5Cl-BTA works slightly better than other tested inhibitors (BTA, TRA and BIA) which points to a better and more efficient adsorption of this inhibitor to the copper containing intermetallic phases when compared to others. The same behaviour is seen for the combinations of this inhibitor with the also tested rare earth metal salts ($Ce(NO_3)_3$) and ($La(NO_3)_3$).

- Different concentrations of the selected inhibitor systems (5Cl-BTA, 5Cl-BTA + Cerium (III) Nitrate and 5Cl-BTA + Lanthanum (III) Nitrate) were systematically analysed in chloride containing media

- It was found that all tested inhibitors with concentrations lower than 0.5 mM lost their corrosion inhibition performance during time.

- Calculations were done in order to numerically assess and estimate the values of the empirical localization corrosion parameter **L** (estimates the dangerousness of the localized corrosion) and the tested inhibitor systems efficiencies (*IE*).

- The relationship between all aspects that can influence the value/character of the localized corrosion attack helped to conclude that high values of $\mathbf{I_{max}}$ **An.** lead to high values of **L**. Although a promising approach the estimation of the **L** index requires for more systematic testing and parameter development in the future.

- It was found that the inhibitor efficiencies (*IE*) for systems containing BTA or 5Cl-BTA are mathematically higher for the case of AA2024. This is related with the more active reference system (0.05M NaCl) of AA2024 when compared to less active AA2198.

- In most of the studied corrosive/inhibitive mediums the AA2198 demonstrates slightly higher corrosion resistance than AA2024.

- Also the study of the effect of inhibitors concentration led to the conclusion that generally the systems under 0.05mM concentration do not show good performance.

7. REFERENCES

[1] Corrosion Basics, An Introduction, L.S. Van Delinder, ed. (Houston, TX: NACE, 1984). (http://www.nace.org/Corrosion-101/#sthash.xLWjvl6K.dpuf) – Acessed on the 10th April.

[2] Pierre R. Roberge, Corrosion Engineering – Principles and Practice, McGraw-Hil, 2008.

[3] Philip A. Schweitzer, Fundamentals of Corrosion – Mechanisms, Causes and Preventative Methods, CRC Press, 2010.

[4] Mário G. S. Ferreira, "Corrosão dos Materiais", Aveiro, 2001.

[5] William D. Callister Jr., Fundamentals of Material Science and Engineering, John Wiley & Sons, Inc., 2008.

[6] Kiryl A. Yasaku, Mikhail L. Zheludkevich, Sviatlana V. Lamaka and Mário G. S. Ferreira, "Mechanism of Corrosion Inhibition of AA2024 by Rare-Earth Compounds", *Journal of Physics and Chemistry*, vol. 110, pp. 5515-5528, 2006

[7] Zhang, W.; Frankel, G. S. *Electrochim Acta* 2003, 48, 1193

[8] Kiryl A. Yasaku, Mikhail. L. Zheludkevich, Sviatlana V. Lamaka and Mário G. S. Ferreira, "Role of intermettallic phases in localized corrosion of AA5083", Electrochimica Acta, vol. 52, pp. 7651-7659, 2007

[9] Sviatlana V. Lamaka, Mikhal L. Zheludkevich, Kiryl A. Yasaku, M. F. Montemor, Mário G. S. Ferreira, "High effective organic corrosion inhibitors for 2024 aluminium alloy", Electrochimica Acta, vol. 52, pp. 7231-7247, 2007

[10] Moreto, J. A., Gamboni, O. C., Marino, C. E. B., Bose Filho, W.W., Fernandes, J. C. S., & Rocha, L. A., (2012). "Comportamento corrosivo de ligas de Al e Al-Li usadas como materiais aeronaúticos". Corrosão e Protecção de Materiais, 31 (3-4), 60-6

[11] K. Nisancioglu (Corrosion of aluminium alloys) in Proceedings of 3rd International Conference on Aluminium Alloys, V. 3, p. 239, Trondheim, Norway (1992).

[12] Mikhail L. Zheludkevich, Kiryl A. Yasaku, S. K. Poznyak, Mário G. S. Ferreira, “Triazole and thiazole derivatives as corrosion inhibitors for AA2024 aluminium alloy”, Corrosion Science, vol. 47, pp. 3368-3383, 2005

[13] Silvar Kallip, Alexandre C. Bastos, Kiryl A. Yasaku, Mikhail L. Zheludkevich, Mário G. S. Ferreira, “Synergistic corrosion inhibitors on galvanically coupled metallic materials”, Electrochemistry Communications, vol. 20, pp. 101-104, 2012.

[14] Kiryl A. Yasakau, J. Tedim, Mikhail L. Zheludkevich, Mário G. S. Ferreira. Smart self-healing coatings for corrosion protection of aluminum alloys, *HandBook of smart coating for materials protection*, 10, 224-274 (2014).

[15] Maria Serdechnova, Silvar Kallip, Mário G.S. Ferreira, Mikhail L. Zheludkevich Active self-healing coating for galvanically coupled multi-material assemblies. *Electrochemistry communications* 41, 51-54 (2014).

[16] C. Scheffey, Rev. Sci. Instrum. 59 (1988) 787

[17] H.S. Isaacs, Y. Ishikawa, in: R. Baboian (Ed.), Electrochemical Techniques for Corrosion Engineering, NACE, Houston, 1986, p. 17.

[18] Alexandre. C. Bastos, S. A. S. Dias, T. C. Diamantino and Mário G. S. Ferreira, “Uma introdução à técnica SVET,” Corros. Prot. Mater., vol. 32, pp. 50-57, 2013.

[19] Yevgen Barsukov and J. Ross Macdonald, “Electrochemical Impedance Spectroscopy”, Characterization of Materials. 1–17, 2012